Accepted Manuscript

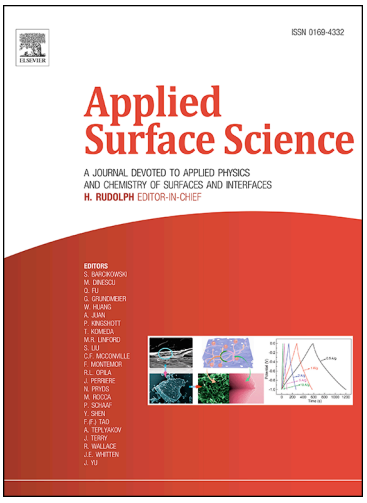

Full Length Article

Graphene films decorated with TiO_2 grown by atomic layer deposition: characterization and photocatalytic activity study under UV-visible light

Francesca Marchetti, Nadhira Laidani, Marina Scarpa, Gloria Gottardi, Enrico Moser

PII: S0169-4332(18)33213-6
DOI: https://doi.org/10.1016/j.apsusc.2018.11.136
Reference: APSUSC 40982

To appear in: *Applied Surface Science*

Received Date: 19 June 2018
Revised Date: 15 November 2018
Accepted Date: 16 November 2018

Please cite this article as: F. Marchetti, N. Laidani, M. Scarpa, G. Gottardi, E. Moser, Graphene films decorated with TiO_2 grown by atomic layer deposition: characterization and photocatalytic activity study under UV-visible light, *Applied Surface Science* (2018), doi: https://doi.org/10.1016/j.apsusc.2018.11.136

GRAPHENE FILMS DECORATED WITH TiO_2 GROWN BY ATOMIC LAYER DEPOSITION: CHARACTERIZATION AND PHOTOCATALYTIC ACTIVITY STUDY UNDER UV-VISIBLE LIGHT

Francesca Marchetti[1,2], Nadhira Laidani[*, 2], Marina Scarpa[1], Gloria Gottardi[2] and Enrico Moser[1]

[1] University of Trento, Department of Physics, Via Sommarive 15, 38123 Povo, Trento, Italy

[2] Center for Materials and Microsystems, Fondazione Bruno Kessler, Via Sommarive 18, 38123 Povo, Trento, Italy

Abstract

The great potential of graphene can be enhanced thanks to the functionalization of its surface. For this aim, different thicknesses of TiO_2 were grown on graphene films by atomic layer deposition (ALD) at 200 °C using H_2O and $TiCl_4$ as precursors. The changes in electronic structure of graphene after the deposition of TiO_2 and the influence of graphene in TiO_2 photocatalytic activity under UV-Visible irradiation were studied. Results indicated the presence of inhomogeneity and intrinsic strain effects within the same sample. Undecorated graphene showed pre-existent strain due to the mismatch between graphene film and the underlying substrate, while non-intentional self-doping is caused by the presence of charged impurities. The deposition of TiO_2 films with thickness ≤10 nm led graphene to be p-doped, while strain became the dominant effect increasing film thickness. Oxygen vacancies in the film decreased exponentially by increasing the film thickness leading to a stoichiometric O/Ti atomic ratio of TiO_2 above 10 nm thickness. The combination of TiO_2 and graphene enhanced the efficiency of electron-hole separation of TiO_2 under UV-Visible light, leading

[*] Corresponding author. Tel: +39 0461 314453, E-Mail: laidani@fbk.eu (Nadhira Laidani)

to a higher photocatalytic activity tested for methyl red molecule degradation, making TiO_2/Graphene hybrid material a promising candidate for the photodegradation of pollutants and water purification.

1. Introduction

Graphene generated great scientific and industrial interest in the last years [1, 2, 3, 4] due to its intrinsic mechanical [5], thermal [6] and electrical [7, 8] properties. Moreover, the functionalization of graphene surface is supposed to enhance its properties [9, 10]. During the past decades, the attention on energy-related and environmental applications (such as photodegradation process of organic pollutants) significantly increased [11, 12]. It has been found that TiO_2 based materials (in particular TiO_2-Carbon materials) have photocatalytic properties for the purification of air and water [11]. In fact, the combination of TiO_2 (or other semiconductor photocatalyst) and graphene gives rise to properties that can facilitate the effective photodegradation of pollutants, such as increasing the efficiency for the electron-hole separation, reducing the recombination of the carriers [12]. TiO_2 is an efficient photocatalyst under UV irradiation, nevertheless TiO_2-Graphene composites can have visible-light photocatalytic activity [12].

For this purpose, atomic layer deposition (ALD) has been employed to deposit TiO_2 onto graphene films. ALD is a thin film growth technique with an exceptional conformality, unique uniformity (also on very large substrate area) and it enables a very high thickness control at atomic level [13, 14]. These characteristics distinguish ALD from other deposition techniques. The deposition is based on the alternation of two self-limiting surface reactions of typically two gaseous reactants, in a layer-by-layer mechanism. Thus, by changing the number of deposition cycles, different TiO_2 film thicknesses can be achieved.

The deposition of TiO_2 onto graphene surface, as well as the presence of defects and dopants in graphene layer, lead to changes in the electronic structure of graphene itself. Monolayer and bilayer graphene have, in fact, a very simple electronic structure. They are defined zero-bandgap semiconductors, because the valence and conduction bands intersect at the Dirac point (i.e. the corner sites of the hexagon of the honeycomb lattice) [15]. Therefore, changes in electronics structure have a fundamental role in determining the characteristics and properties of graphene [16]. Raman spectroscopy represents a very important tool for the characterization of the electronic structure of graphene.

For what concerns the analysis of the surface chemistry, X-Ray Photoelectron Spectroscopy (XPS) has been performed. XPS gives information about the elemental composition, stoichiometry, chemical and electronic states of the elements that exists within the samples materials.

2. Experimental details

2.1 Graphene film

Monolayer graphene film on Si/SiO_2 4" wafer is provided by *Graphenea*. Graphene film has been produced by chemical vapor deposition (CVD) and transferred to a circular substrate of Si/SiO_2 (300 nm) by a wet transfer process. The growth of graphene was performed via CVD method using 18 μm thick copper (Cu) foil as catalyst and methane as carbon source. Graphene layer was protected by polymethyl methacrylate (PMMA) as sacrificial layer before the transfer. A ferric chloride solution was then used for the copper etching in order to remove the Cu foil. At this point graphene was transferred via PMMA assisted wet transfer process and once the etching was complete, graphene was washed in deionized water and transferred onto the final substrate. The PMMA layer was removed with solvents (acetone and isopropyl alcohol) and then dried with a nitrogen (N_2) flux.

2.2 TiO_2 thin films deposition by ALD

TiO_2 films were grown on graphene films (Graphenea) and on silicon substrates (n-doped silicon wafer (phosphorous), with orientation <100>, resistivity > 10 Ω·cm, wafer thickness 450 μm and native oxide thickness ~1 nm) by atomic layer deposition, in a *Beneq TFS500nSILVER®* ALD instrument, with titanium tetrachloride ($TiCl_4$) (99.995%) and water as precursors.

Prior to load the samples in the ALD reactor, graphene films and silicon substrates were ultrasonically cleaned with deionized water for 1 minute, acetone and isopropanol alcohol for 5 minutes each. After each sonication phase, the samples are flushed with nitrogen (N_2) gas. Only graphene films were then heated at 250°C for 1 hour in the oven in order to remove the carbon based organic residues and absorbants such as H_2O [17].

The thin film growth was performed at 200°C with 80°C pre-heating of the reactor, while the procedures were set as follows: (1) a 500 ms $TiCl_4$ pulse, (2) a 1000 ms purge of oversupplied titanium tetrachloride and any gaseous by-products, (3) a 250 ms water pulse and (4) a 750 ms purge of oversupplied water and by-products. These steps sequence constitute a single ALD-TiO_2 cycle and the estimated growth per cycle is 0.067 nm. In this study, TiO_2 films are obtained with 7, 15, 30, 75, 105, 150, 375, 750 and 1125 cycles (which correspond to the following nominal film thicknesses: 0.5 nm, 1 nm, 2 nm, 5 nm, 7 nm, 10 nm, 25 nm, 50 nm and 75 nm respectively).

2.3 Raman Characterization

To study defects and dopants in the samples, TiO_2-Graphene hybrid materials were characterized by Raman spectroscopy. For the spectra acquisition *Aramis* Micro-Raman spectrograph with red laser (wavelength 632.8 nm and excitation energy 1.96 eV) has been

employed. The 100x objective used has numerical aperture 1 and working distance 0.21 mm, which offered a high resolution.

Because perfect graphene surface is chemically inert, ALD films might nucleate only at specific defect sites [14, 18, 19]. Both the irregular distribution of the graphene film onto the substrate and the possible nucleation of TiO_2 that starts at specific defect sites, lead to inhomogeneity of the sample surface. The possible inhomogeneity makes necessary the acquisition of about 20 spectra per sample at different surface coordinates, in order to obtain a distribution of the Raman characteristic peak parameters for each sample.

2.4 XPS Characterization

TiO_2-Graphene samples were analyzed with Scienta ESCA 200 spectrometer with a monochromatic Al Kα X-ray source (1486.6 eV). The spectra of C1s, O1s, Si2p, Ti2p core lines and valence band (VB) were acquired at 150 eV pass energy (resolution 0.4 eV). Because the electrostatic charging of the surfaces, the spectra were corrected for the binding energy shift using the binding energy of C1s (285 eV) as reference, which corresponds to C-H signal due to hydrocarbon contamination. All the binding energies were given with respect to the Fermi level and the core line spectra were fitted with a Gauss-Lorentz peak shape, after a Shirley-type background subtraction. In the case of the valence band only a fit of the Ti3d state was performed. Moreover, the chemical composition, as well oxide stoichiometry, were derived by applying the Scienta sensitivity factors for the different core levels.

The fitting software used for the X-Ray Photoelectron Spectroscopy (XPS) analysis is based on RStudio, which is a free and open-source integrated development environment (IDE) for R, a programming language for statistical computing and graphics. The software was internally developed.

2.5 Atomic Force Microscopy (AFM)

The surface topography of the TiO_2/Graphene sample obtained with 1125 ALD cycles was examined using atomic force microcopy (AFM) (AFM NT-MDT P47H apparatus) in contact mode.

2.6 Photocatalytic activity

The photocatalytic activity of graphene film and of TiO_2 layer deposited both on graphene and silicon substrate has been tested. The photocatalytic activity was investigated by following the kinetic of degradation of methyl red. This dye is considered a reference molecule for the tests of photocatalytic degradation of pollutants. For this reason, the optical spectra of the dye [20] and the degradation products have been carefully characterized [21].

The tests were performed in quartz cuvettes, which are transparent in the UV-Visible range. Each cuvette contained 2.55 mL of a solution of 16 µM methyl red in 8 mM Tris-HCl buffer (pH 8.2) and the sample with a superficial area in the range of 1 cm^2.

The cuvettes containing sample and methyl red were placed under a solar simulator, which has been set at the irradiation power of 1 sun (i.e. 1 KW/m^2). They were laid under the sun light over a waving platform shaker to allow the solution to come in contact with the active surface, which is perpendicular to the light beam.

After regular time intervals, the absorption spectra of the methyl red solution inside each cuvette are acquired in the UV-Visible range (200-800 nm) using a *Cary 100* spectrophotometer. The absorbance value at 430 nm was taken in exam, for each spectrum, to follow the kinetic of degradation of the dye.

3. Results and discussion

3.1 Raman Characterization

3.1.1 Peaks identification

Figure 1 shows a representative Raman spectrum of graphene film decorated with TiO_2 (1125 ALD cycles, 75 nm nominal thickness) in the range from 100-3000 cm^{-1}.

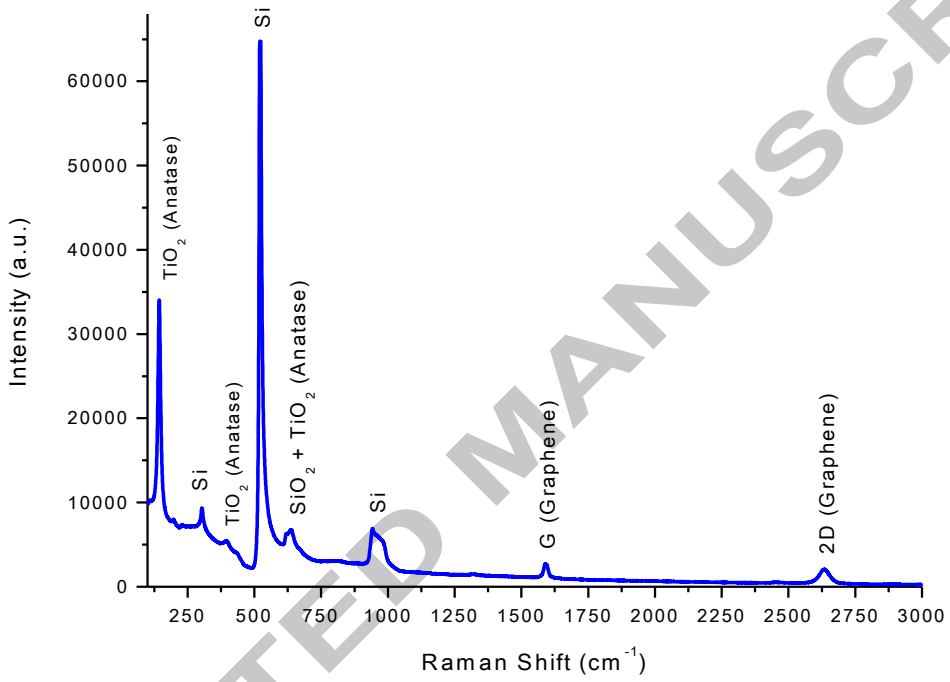

Figure 1: Raman spectrum in the wavenumber region from 100-3000 cm^{-1} showing the peaks of TiO_2 anatase phase (obtained with 1125 ALD cycles, 75 nm nominal thickness), silicon peaks (originated in the substrate on which graphene has been deposited) and graphene peaks.

The peaks of silicon and SiO_2 (at ~300 cm^{-1}, ~522 cm^{-1}, ~630 cm^{-1} and ~950 cm^{-1}) are related to the substrate on which graphene has been deposited. The TiO_2 anatase phase peaks are at ~142 cm^{-1} (E_g), ~390 cm^{-1} (B_{1g}) and ~640 cm^{-1} (E_g) [22] and they are visible only for film thicknesses obtained with a number of cycles ≥ 375 (25 nm nominal thickness) (Figure 2) [23]. Nevertheless, the presence of TiO_2 was confirmed by the XPS analysis (see next section).

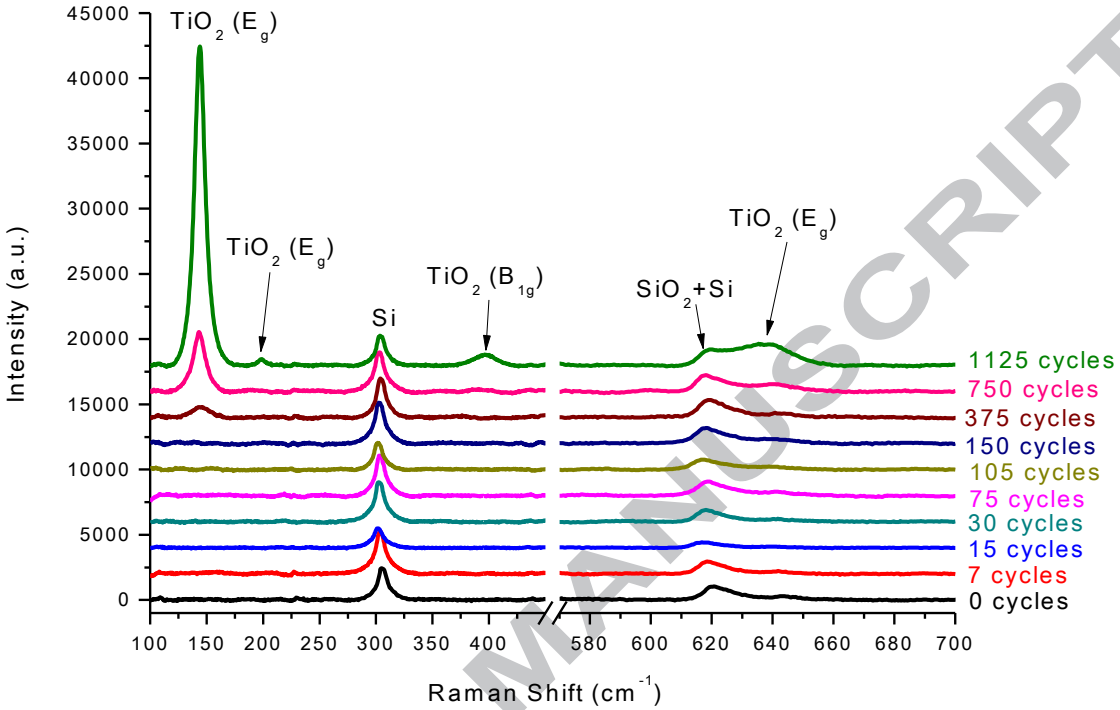

Figure 2: Raman spectra of TiO_2 in range from 100-700 cm^{-1}. The TiO_2 anatase phase peaks appear only for films obtained with a number of cycles higher than 150 ALD cycles.

This phenomenon is related to the fact that the crystallinity of the materials, deposited by ALD, depends on several factors, such as: deposition temperature, type of reactants, presence of impurities, substrates, film thickness, etc. [13]. Perfect graphene surface is chemically inert so the TiO_2 film might nucleate only at specific defect sites [14, 18, 19]. Thus, thinner films of TiO_2 appeared amorphous and became crystalline when a thickness greater than 10 nm is reached [13, 23]. For TiO_2 there is the growth of an initially amorphous film, in which crystalline nuclei can form randomly [13] (the quantity of crystalline phase is not enough to be detected by Raman spectroscopy). These crystalline grains can grow when more material is deposited and the crystallization of the previous amorphous film next to the grains occurs [13]. Anatase crystalline phase is present, while rutile phase can not be detected. In fact,

anatase phase generally is observed for film grown at 165-350°C, while rutile phase dominates for higher temperatures (> 350°C) [23].

The characteristic Raman peaks of graphene can be identified by considering the Raman shift range from 1200-3000 cm^{-1} (Figure 3). From the Raman spectrum: D peak at ~1330 cm^{-1}, characteristic G and 2D bands at ~1590 cm^{-1} and ~2630 cm^{-1} respectively, and also G* peak at ~2460 cm^{-1} were visible. The degree of disorder and the density of defects can be quantified by studying the intensity of the D peak [16, 24, 25, 26, 27], which is generated from a second order process due to an in-plane breathing-mode of the carbon rings, that involves one iTO phonon and one defect [16, 28]. On the other hand, doping was investigated considering the variations in G and 2D bands [16, 26, 29, 30]. The G peak is connected to the in-plane sp^2 carbon-carbon stretching (iTO and iLO) phonon modes at the center of the 1^{st} Brillouin zone and comes from a normal first order Raman scattering process [16, 28]. While the 2D peak is generated by a second order process due to an in-plane breathing-mode (like the D band), which involves two iTO phonons instead [16, 28]. The G* peak at about 2460 cm^{-1} (for the red laser with energy 1.96 eV) was also visible, it can be explained by the double resonance Raman model with an intervalley process (as 2D band) which involves one ITO and one LA (longitudinal acoustic) phonon [28].

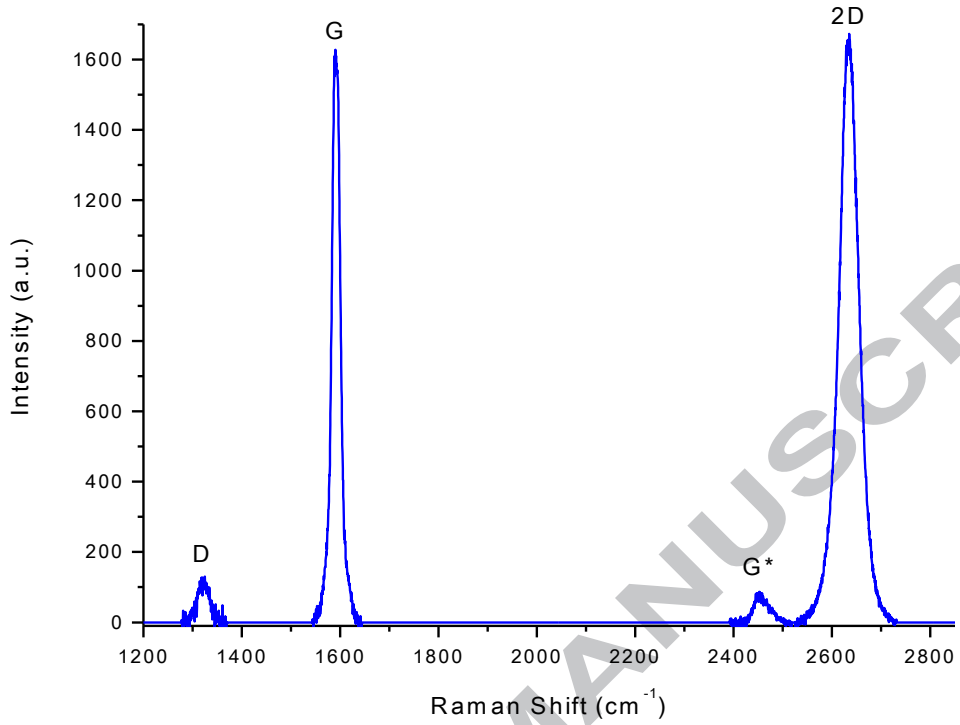

Figure 3: Characteristic Raman peaks of graphene in the wavenumber region from 1200-3000 cm^{-1} (sample of graphene decorated with TiO_2 film obtained with 1125 ALD cycles) showing the D, G, G* and 2D peaks at ~1330 cm^{-1}, ~1580 cm^{-1}, ~2460 cm^{-1} and ~2650 cm^{-1} respectively.

3.1.2 Doping effect analysis

The presence of dopants, as well as that of defects, is responsible of changes in intensity, position and full width at half maximum (FWHM) of the characteristic Raman peaks [16]. For all the graphene samples (with and without deposited TiO_2), differences in the peak position, FWHM and ratio between the D- and G- peak intensities were determined considering the same sample at different surface coordinates, indicating that inhomogeneous doping and self-doping (in the case of graphene sample) could happen [2].

Figure 4 shows the values of FWHM and position of the G peak for the same graphene sample without TiO_2 at different surface coordinates. The data points represent measurements made at different locations on the surface of the same sample.

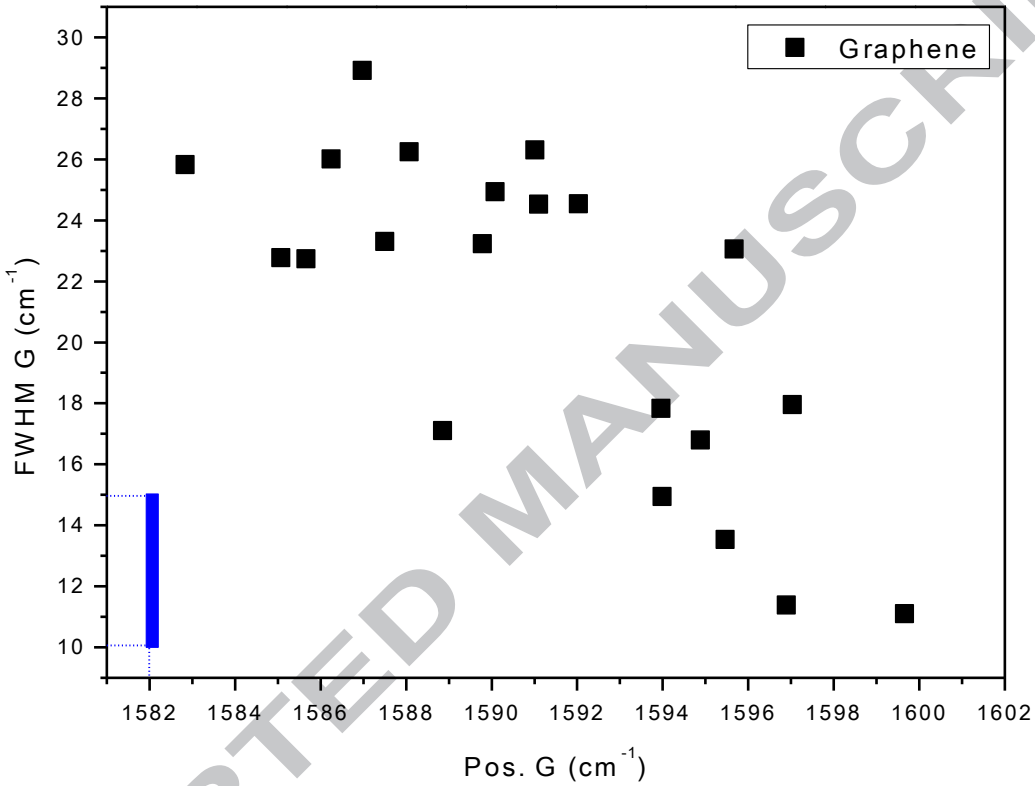

Figure 4: Values of FWHM of G band in function of the position of G peak for graphene sample. The values are obtained from the Raman spectra acquired at different points on the same graphene sample surface without TiO_2. The blue region was added to the plot to better visualize the parameters range for ideal mono-layer graphene [28, 31].

From the distribution of the values, it is clear that the sample was not uniform. In particular, the values of FWHM are in the range of 10-30 cm^{-1}, while the G band position ranges between 1582 cm^{-1} and 1600 cm^{-1}. For a mono - layer graphene, the width of the G peak is around 10-15 cm^{-1} [31], while the typical G band position is around 1582 cm^{-1} [28] (the typical values for mono–layer graphene lay within the blue bar in Figure 4). These differences with respect to the expected ones for graphene can be related to several phenomena: self-doping process [29, 32], structural disorder [30, 33, 34] and strain due to the

lattice mismatch of graphene film with the underlying substrate [31, 34, 35, 36]. Differently from other characteristic Raman peaks, the intensity of the G band of graphene is almost constant as a function of disorder [2] and both its position and FWHM are not influenced by the number of layers [37], but its position blue-shifts significantly [29] and its FWHM decreases [2] by either p or n doping. Graphene is strongly influenced by the underlying substrate [38] and the charged impurities of SiO_2/Si substrate (on which graphene film has been deposited) lead to unintentional doping in graphene [34]. Therefore the weak doping effect from the SiO_2 substrate is evidenced by a blue-shift of the G band from 1582 cm^{-1} to 1600 cm^{-1} [39], but also from the decrement of its FWHM [2] (shown in Figure 4). On the other hand, the large values of FWHM G above 18 cm^{-1}, when the position of G peak is in the range of 1582-1592 cm^{-1}, can be ascribed to the influence of structural disorder [30, 33, 40]. In fact, the plot of FWHM G as a function of I_D/I_G (Figure 5), where I_D/I_G ratio gives information about the degree of structural disorder, shows that the values of FWHM G > 18 cm^{-1} are observed for $I_D/I_G \geq 0.4$, i.e. where the degree of structural disorder becomes important [30, 34, 39].

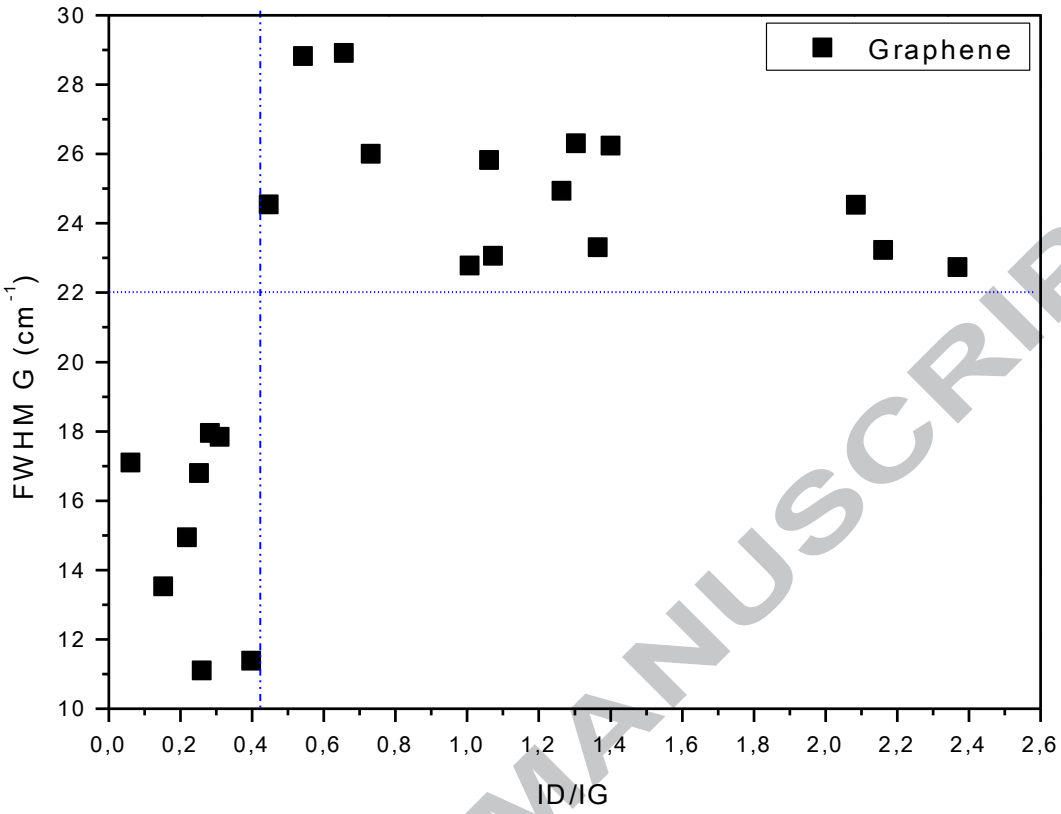

Figure 5: Values of FWHM of G band in function of the I_D/I_G ratio for graphene sample. The values are obtained from the Raman spectra acquired at different points on the same graphene sample surface without TiO_2. I_D/I_G ratio represents the degree of structural disorder.

If we consider all the (Pos. G, FWHM G) data points in Figure 4 related to graphene sample and starting from the surface point with the lowest Pos. G value, at ~1582 cm^{-1}, one can see the influence of structural disorder that makes the corresponding FWHM G as high as ~26 cm^{-1}. Further, by sorting the Pos. G values ascending, a decrease of FWHM G (with respect to the previous value) can be noticed and ascribed to the doping effect due to SiO_2 substrate.

When TiO_2 films were grown onto graphene surface, changes in the characteristic Raman peaks of graphene occurred. Figure 6 shows the plot of the FWHM of G in function of G peak position of the TiO_2/Graphene samples obtained with different numbers of cycles by ALD. The data related to graphene are indicated for comparison.

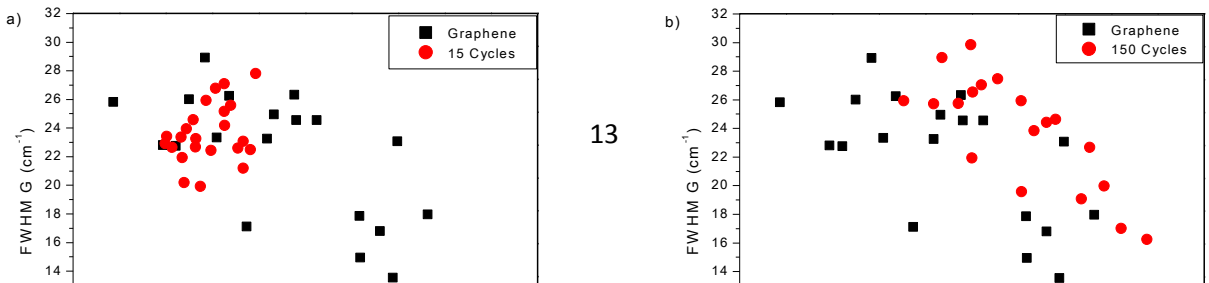

Figure 6: Distribution of FWHM of G band as function of the position of G peak. Comparison between undoped graphene (black) and TiO_2-Graphene hybrid material (red) obtained with: a) 15 ALD deposition cycles, b) 150 cycles and c) 750 cycles.

For 15 deposition cycles (Figure 6a), the distribution of the data points on the same sample surface is more uniform with respect to the graphene sample. The values are, in fact, concentrated at high FWHM and low G band position values, in a smaller range of values than graphene film. This means that the strain in graphene is higher [30, 31] when a thin TiO_2 film is deposited onto graphene. The same trend was observed for the films obtained with 15, 30 and 75 ALD cycles (not shown).

Considering the TiO_2/Graphene sample obtained with 150 cycles (Figure 6b), the distribution of the values is similar to that obtained for the graphene sample. Nevertheless, even though the values of FWHM span the same range for both samples, the G peak position values are higher. This distribution shows that increasing the number of ALD cycles (and so the thickness of the TiO_2 film), the strain was still present as indicated by data points with

FWHM of G ~26 cm^{-1}, but for higher values of Pos. G an effect of doping also appears [30, 31], since the position of the G peak is upshifted. This evolution trend was also observed for films obtained with 105 and 375 cycles (not shown).

Increasing the thickness of TiO_2 by depositing 750 cycles (Figure 6c) the distribution of the values are grouped in the same region, with smaller FWHM values and higher G peak position with respect to the other samples decorated with a lower number of cycles.

Therefore, increasing the number of ALD cycles, the FWHM of G peak decreases, while the position of the G band increases. This trend indicates that increasing the number of ALD cycles a doping process could happen [26, 30, 31, 34], however the upshift of the G peak position can also be ascribed to strain [36, 41]. The behavior of FWHM and position of the G peak can inform about doping occurrence, but it does not allow to distinguish between p- or n- doping processes. In order to understand if the deposition of TiO_2 leads to p- or n- doping process, the relation between 2D and G peaks position has to be considered [16]. The position of the G peak upshifts for both n and p doping, while the 2D band position increases (decreases) if the hole (electron) concentration increases instead [16, 42]. Moreover, it is possible to discriminate between doping and strain by focusing on the variation of the 2D peak position in function of the variation in the G-band position (i.e. $\frac{\partial Pos2D}{\partial PosG}$ ratio) [43]. Values of $\frac{\partial Pos2D}{\partial PosG} < |0.8|$ indicate doping [44], otherwise $\frac{\partial Pos2D}{\partial PosG} \sim |2.5|$ signifies (only) mechanical strain [44, 45, 46].

Figure 7 shows the comparison between the position of 2D vs position of G peaks of graphene sample (without TiO_2) and of TiO_2/Graphene samples obtained with different number of cycles by ALD. While Table 1 reports for each sample the values of $\frac{\partial Pos2D}{\partial PosG}$ ratio, taken as the slope of a linear fit with 95% confidence level for parameters.

Number of ALD cycles	$\frac{\partial Pos2D}{\partial PosG}$
0	-0.3
7	0.04
15	0.06
30	0.2
75	0.3
105	0.03
150	0.1
375	0.03
750	1.4
1125	1.5

Table 1: Variation of the 2D peak position as a function of the variation in the G-band position (i.e. $\frac{\partial Pos2D}{\partial PosG}$) for all samples.

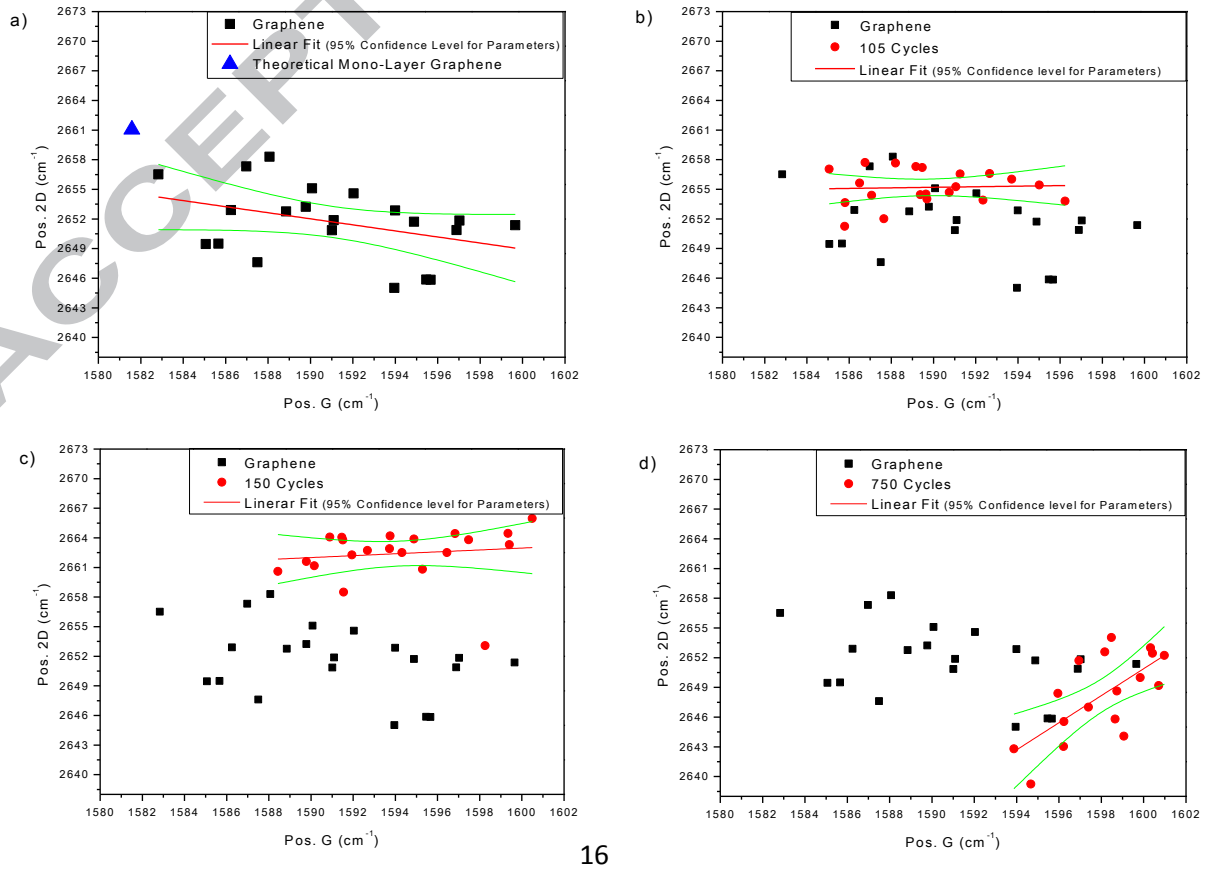

Figure 7: Distribution of 2D band position as function of the G peak position. a) untreated graphene sample (black squares) with the data point corresponding to the theoretical mono-layer graphene (blue triangle). The comparison between untreated graphene (black squares) and TiO_2-Graphene hybrid material (red dots) obtained with: b) 105 ALD deposition cycles, c) 150 cycles and d) 750 cycles were also reported. For each sample, the linear fit with 95% confidence level for parameters was plotted. The $\frac{\partial Pos2D}{\partial PosG}$ ratio represents the slope of the linear fit.

Comparing the distribution of the position of the 2D peak as a function of the G peak for different surface locations onto graphene sample and a TiO_2/Graphene one obtained with 105 cycles (Figure 7a and 7b), we can see that no evident strain effect is present [35, 44, 45]. In fact, the $\frac{\partial Pos2D}{\partial PosG}$ (on the same sample) is (-0.3) in the case of graphene sample and 0.03 for TiO_2/Graphene obtained with 105 cycles (Table 1). The negative value for graphene is due to the fact that the 2D peak position was decreasing when the position of the G peak was increasing, and it is ascribed to n-doping [16, 42, 47]. This n-type behavior is intrinsic to the SiO_2/graphene interface (that is, surface states on SiO_2 are donating electrons to the graphene) [17]. If water molecules or other contaminants coming from the atmosphere were absorbed on the surface of graphene after the cleaning procedure of the samples, p-type doping of graphene would have been expected [17, 48], which does not seem here to be the dominant effect, if any. The positive value of the $\frac{\partial Pos2D}{\partial PosG}$ for TiO_2/Graphene is ascribed to p-doping of graphene [16, 42] induced by TiO_2 [49] even though it can be also related to H_2O absorption [17, 50, 51], since water is one of the two ALD precursors used for TiO_2 deposition. Moreover, we can see that generally the distribution of the Pos. 2D values in the case of TiO_2/Graphene sample is slightly higher than those for graphene. This trend is similar

for all graphene samples coated with a number of ALD cycles ≤ 105 and it can indicate a p-doping process [16].

Increasing the number of cycles (Figure 7c), we can see that for TiO_2/Graphene sample obtained with 150 cycles (similarly for the decoration with 375 cycles) there is no evident strain effect, since $\frac{\partial Pos2D}{\partial PosG}$ is equal to 0.1 and 0.03 for the samples decorated with 150 and 375 TiO_2 cycles respectively (Table 1). The distribution of the data points for these two samples span a higher values range with respect to graphene sample (similarly to the previous case) indicating that p-doping process occurred [16].

A completely different situation appears for higher number of cycles (≥ 750 cycles) (Figure 7d). In fact, in this case the $\frac{\partial Pos2D}{\partial PosG}$ ratio is equal to 1.4, which is much higher than what found before and it indicates that p-doping and strain were both present [35, 45] and the second one represents the dominant effect. In fact, the film thickness is not expected to modify the doping level (the p-doping of graphene occurred through an interface charge transfer from graphene to titanium oxide), in contrast with the stress related to the film growth which is expected to increase with the film growth, till eventually dominating the Raman spectra features.

3.1.3 Analysis of defects

The presence of defects, as well as that of dopants, is responsible for the changes in Raman peak parameters. When defects are present, the intensity of the D peak (I_D) increases relatively to that of G peak (I_G) [16]. The I_D/I_G ratio gives information also about the crystallite size (L_a) of graphene according to the following Tuinstra-Koenig relation [2, 16]:

$$\frac{I_D}{I_G} = \frac{C(E_L)}{L_a[nm]}$$

Where $C(E_L)$ depends on the laser excitation energy (E_L) and its value is $C(E_L)$ ~38 nm for the red laser [16].

Figure 8 shows the graphs of L_a in function of ALD cycles.

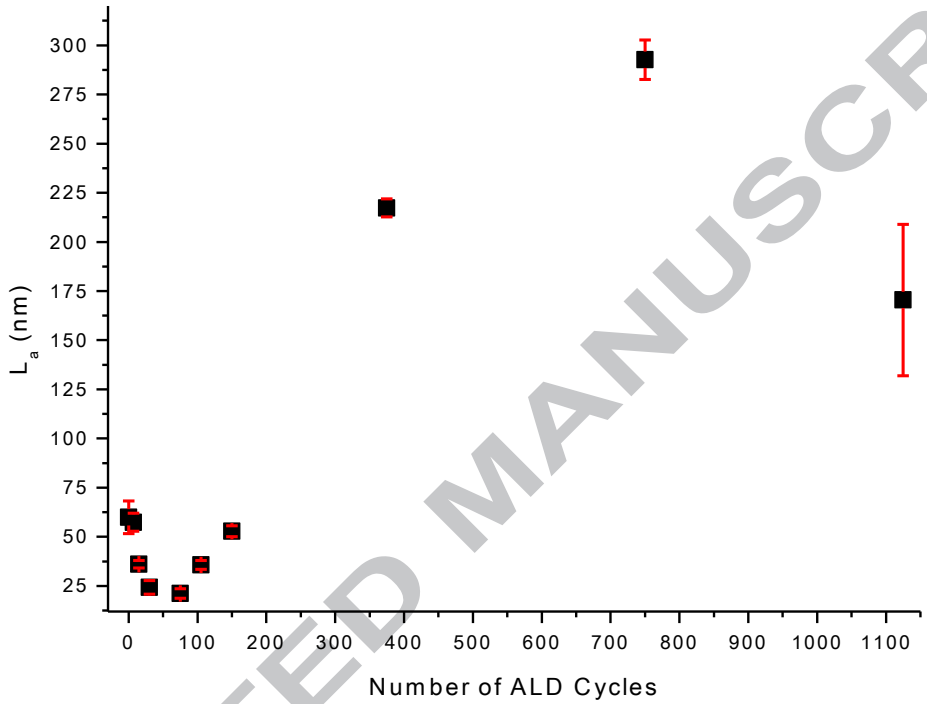

Figure 8: L_a mean value of each sample vs number of cycles used for the TiO_2 film deposition.

In particular, L_a decreases (with respect to graphene) when TiO_2 is deposited with a number of cycles ≤ 75, while it increases (but still smaller than for graphene) for a number of cycles between 75 and 150. This means that in the range of 7 and 150 cycles, the growth of TiO_2 reduced the crystalline size indicating a contraction of the graphene lattice. A contraction of the lattice is related to higher hole concentration [26] and thus to a p-doping process of the graphene sample in this range of number of ALD cycles, which is consistent with what was found from the analysis of the G and 2D peak positions.

On the other hand, considering TiO_2 films obtained with a number of cycles higher than 150, L_a becomes considerably high with respect to that of pristine graphene. Therefore, the increase in the crystallite size indicates an expansion of the graphene crystal lattice. This phenomenon is related to the tensile strain effect, which is dominant for higher number of deposition cycles and it is consistent with the $\frac{\partial Pos2D}{\partial PosG}$ values found from the analysis of the positions of G and 2D peaks. The chemical inert surface of graphene might lead the nucleation of TiO_2 only at specific defect sites [18, 19] leading to a partially coated surface. Therefore, the decoration of graphene films would not be uniform from the very first ALD deposition cycles and the tensile strain, observed for the samples coated with a number of cycles higher than 150, can be consistent with the coalescence of the nuclei of deposited TiO_2 [52, 53, 54, 55]. Nuclei formation and coalescence, which is also responsible of the non-homogeneity of TiO_2 film, can be appreciated in Figure 9 which is an atomic force microscopy (AFM) image for the sample decorated with 1125 ALD cycles.

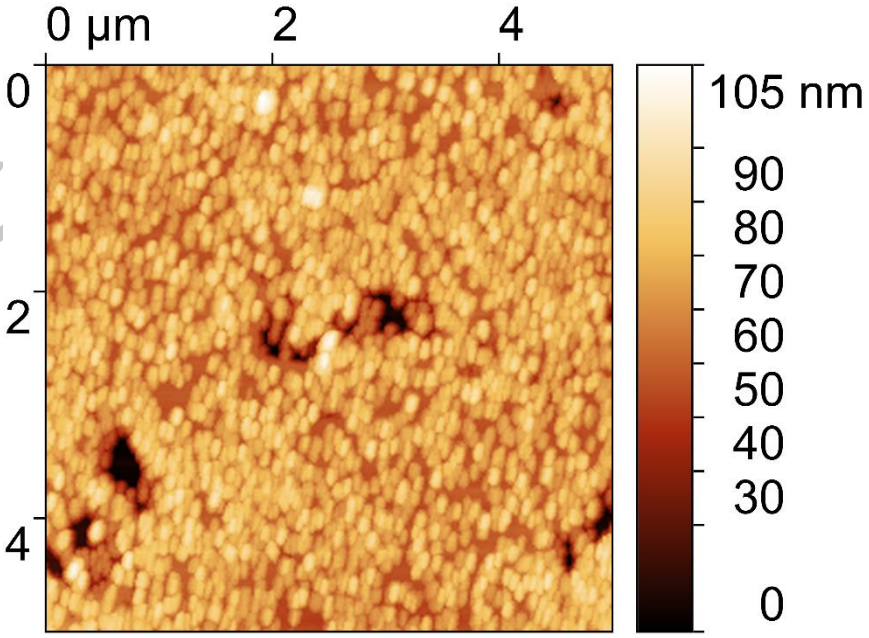

Figure 9: AFM image for the TiO_2/Graphene sample obtained with 1125 ALD cycles (75 nm nominal film thickness)

The AFM image clearly shows the topography of the sample surface. The brighter regions confirmed the presence of grains, while the more uniform areas in between (at about 65 nm height) represented their coalescence. Since the height between the darker and the brighter areas is about 105 nm (but the nominal film thickness of the film should be around 75 nm), the black regions can be ascribed to pinholes able to reach the SiO_2 substrate under the graphene film. These pinholes were consistent with the detection of the SiO_2 signal in XPS spectra also for thicker TiO_2 films (as discussed in the next section). However, further study will be performed in order to completely understand this coalescence mechanism.

3.2 XPS Characterization

X-Ray Photoelectron Spectroscopy (XPS) was used to identify, quantify and determine the stoichiometry of the different chemical elements present on the sample surface.

3.2.1 Elemental analysis

The C1s spectrum (Figure 10 shows that for Graphene film on the left and that for TiO_2/Graphene 375 ALD cycles on the right) is composed by four components. The main peak at 285 eV (C2) (taken as reference) is ascribed to C-H and its presence is due to hydrocarbon contamination. Component C1 at 284.48 eV and 284.02 eV respectively represents the C-C (sp^2) bond of graphene, while component C3 and C4 (at 286.85 eV and 289.14 eV respectively) are due to C-O-C bonds (C3) and O-C=O groups (C4). Components C2, C3 and C4 are ascribed to the interaction of the sample surface with environment.

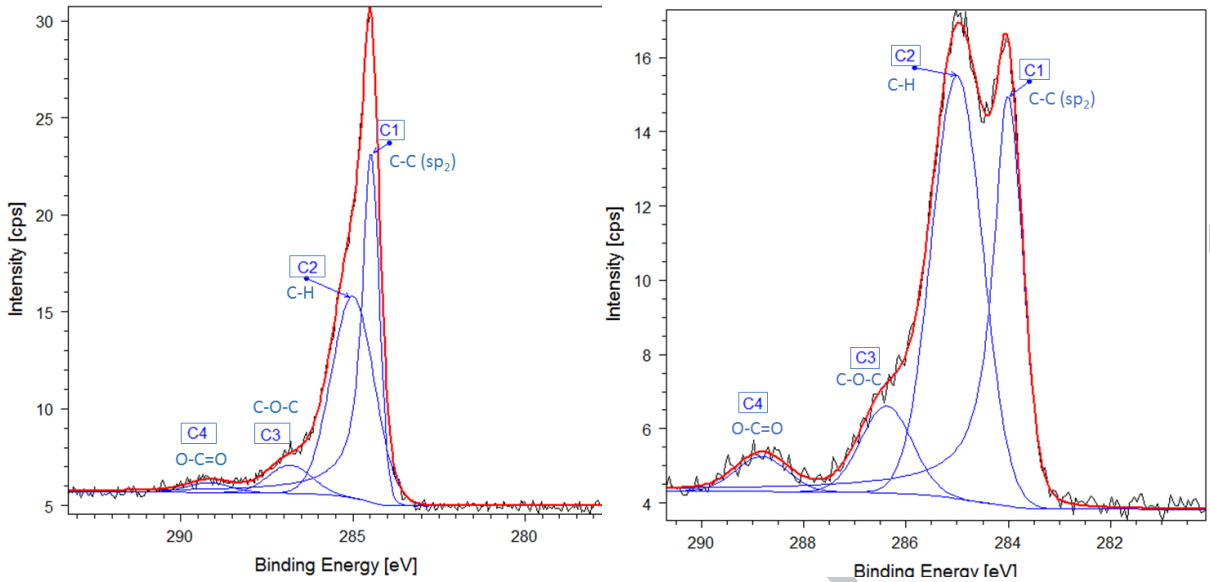

Figure 10: XPS C1s spectrum of untreated graphene film (on the left) and graphene film decorated with TiO_2 with 375 ALD cycles (on the right).

The Ti2p core line spectrum (that of the sample obtained with 375 cycles is reported in Figure 11) consists in two $Ti2p_{3/2}$ (Ti1 and Ti2) and two $Ti2p_{1/2}$ (Ti3 and Ti4) peaks. Ti2 and Ti4, at 458.77 eV and 464.47 eV respectively, are reported in literature as Ti^{4+} states of TiO_2 [56].

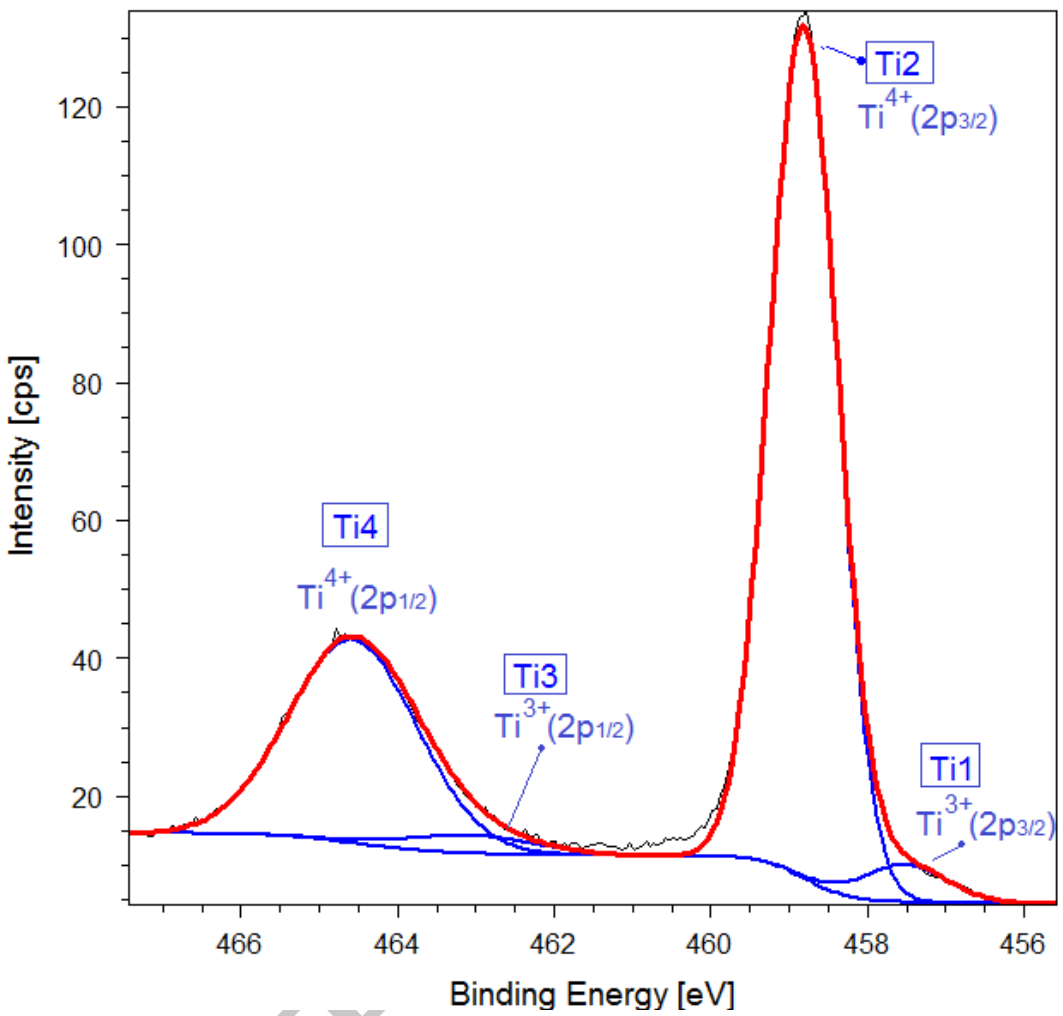

Figure 11: XPS Ti2p spectrum of graphene film decorated with TiO_2 with 375 ALD cycles.

In Table 2, the binding energy values of Ti2 component for all the films are given. We can see that the binding energy of Ti2 component (Ti^{4+} states) for the first deposition cycles (i.e. 7 cycles) is ~ 459.2 eV, which is slightly higher with respect to the tabulated value (~ 458.7 eV [57]).

Number of	C_{C-C}	$Ti^{4+}2p_{3/2}$	$Ti^{3+}2p_{3/2}$	O_{O-Ti}	O_{O-Ti}/Ti	Ti^{3+}/Ti^{4+}	"x"

ALD cycles	BE (eV)	BE (eV)	BE (eV)	BE (eV)	atomic ratio	atomic ratio	in TiO_{2-x}
0	284.48	--	--	--	--	--	--
7	284.17	459.22	457.92	530.61	1.67 ± 0.04	0.18 ± 0.01	0.33 ± 0.04
15	284.06	459.15	457.85	530.62	1.69 ± 0.03	0.11 ± 0.01	0.31 ± 0.03
30	283.99	459.03	457.73	530.44	1.91 ± 0.02	0.10 ± 0.01	0.09 ± 0.02
75	283.95	458.63	457.33	530.13	1.93 ± 0.01	0.05 ± 0.01	0.07 ± 0.01
105	283.87	458.83	457.53	530.16	1.97 ± 0.01	0.05 ± 0.01	0.03 ± 0.01
150	283.97	458.76	457.46	530.22	1.98 ± 0.01	0.05 ± 0.01	0.02 ± 0.01
375	284.02	458.77	457.47	530.22	1.97 ± 0.01	0.05 ± 0.01	0.03 ± 0.01
750	283.86	458.72	457.42	530.05	1.99 ± 0.01	0.05 ± 0.01	0.01 ± 0.01
1125	283.85	458.74	457.44	529.97	1.99 ± 0.01	0.04 ± 0.01	0.01 ± 0.01

Table 2: Number of ALD cycles used to decorate graphene films with TiO_2, C_{C-C} (sp^2), $Ti^{4+}2p_{3/2}$, $Ti^{3+}2p_{3/2}$, O_{O-Ti} binding energies (BE), O_{O-Ti}/Ti, Ti^{3+}/Ti^{4+} atomic ratios and deviation "x" from the ideal stoichiometry in TiO_{2-x}.

On the other hand, components Ti1 and Ti3 at 457.47 eV and 463.17 eV respectively are necessary to have a good fit. In literature these components are attributed to the Ti^{3+} states and they can be related to the presence of point defects in TiO_2 (such as oxygen vacancies) [56] or to Ti_2O_3 phase [58]. The origin of Ti^{3+} states is not fully understood [59, 60]. Ti^{3+} is mainly found near the graphene interface (as reported in next section), it is very likely to be a nucleation or interfacial effect, since the growth of the first few monolayers is different than that of other layers [59, 61]. In fact, graphene is chemical inert and the nucleation of TiO_2 can start at specific defect sites [14, 18, 19]. Since water is one of the precursors used for the ALD process, oxygen and hydroxyl (OH) groups can likely be attached to defect site (such as point defects or boundary defects) of graphene [62] in the very first cycles. Here titanium can easily nucleate forming Ti-OH bonds, which lead to oxygen vacancies in nucleated TiO_2 [59, 63]. Consequently, a very large deviation from the ideal titania stoichiometry was observed (see next section). Both Ti^{4+} and Ti^{3+} states are present whatever the TiO_2 film thickness is.

For what concerns the O1s spectra (Figure 12 reports that of TiO_2/Graphene obtained with 375 cycles), they can be decomposed in three components. The first one (O1) at 530.22 eV corresponds to O-Ti bonds in the titanium dioxide [57], O2 (at 531.27 eV) can be related to

C-O-C groups, to oxygen in a Ti_2O_3 phase [64, 65] but also to Ti-OH groups [59], while the third component (O3 at 532.6 eV) is ascribed to the SiO_2 substrate [57].

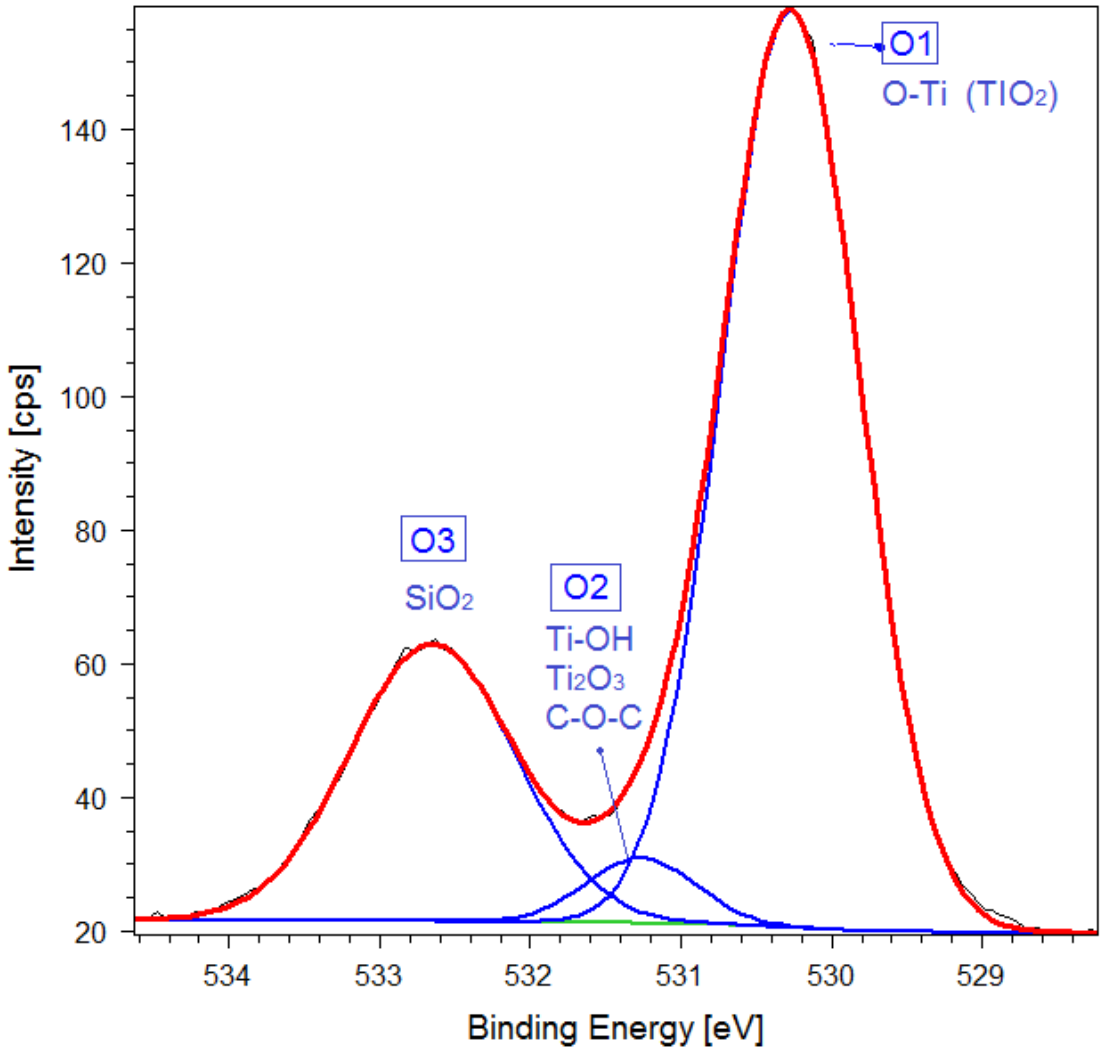

Figure 12: XPS O1s spectrum of graphene film decorated with TiO_2 with 375 ALD cycles.

In Table 2 shows the binding energies of C_{C-C} (sp^2), $Ti^{4+}2p_{3/2}$, $Ti^{3+}2p_{3/2}$ and oxygen peak due to O-Ti bonds (i.e. O1 component), for the different number of ALD cycles.

From this table, we can notice that the C1s spectrum for the untreated graphene film has the C_{C-C} peak related to sp^2 structure centered at binding energy of 284.48 eV. After deposition of TiO_2, a gradual shift of C1s peak toward lower binding energy was observed, reaching a

maximum peak shift by -0.6 eV, with increasing TiO_2 thickness. This shift to lower values constitutes a further proof for p-doping of graphene induced by TiO_2 deposition [49], as also observed by Raman analysis. By forming a physical contact between TiO_2 thin film and graphene, the large work function difference between TiO_2 (~5.1 eV) [66, 67] and graphene (4.0 - 4.4 eV) [68] leads to significant electron transfer from graphene to titania. This results in a hole doping in graphene [49, 68], due to Fermi level alignment [68, 69] and the consequent band bending [70] across the interface. The effect of the electron transfer from graphene to TiO_2, as well as the modification in the Fermi level and the band banding, is also reflected in the higher binding energy of the Ti^{4+} state peak of the Ti2p core line with respect to the tabulated value [68, 71], for the TiO_2 films obtained with 7, 15 and 30 deposition cycles (Table 2). In fact, the XPS binding energy value for all elements core lines is referred to the Fermi energy level. For the samples coated with more ALD cycles, the position of the peak ascribed to Ti^{4+} state is ~ 458.7 eV instead, which is consistent with the tabulated one. Since the average escape depth of a Ti2p photoelectron for an XPS measurement in TiO_2 is about 8 nm (taken as three times the inelastic mean free path determined for a bulk TiO_2 using NIST database [72]), the signal acquired for the samples coated with more than 150 cycles (i.e. with nominal film thickness $\geq$ 10 nm) refers to the more uniform TiO_2 film rather than to the layers close to the interface, which are too far from the surface to be sampled and where charge transfer and bend bending occurs.

3.2.2 TiO_2 Stoichiometry

In order to determine the stoichiometry of TiO_2 the $O_{O\text{-}Ti}$/Ti atomic ratio was considered. The $O_{O\text{-}Ti}$/Ti atomic ratios are determined, for each sample, taking the area under the O1 component of the O1s spectrum and the area under the whole Ti2p spectrum corrected with the sensitivity factors of the instrument for each element. The Ti^{3+}/Ti^{4+} atomic ratios,

determined from the Ti2p spectrum analysis, and the deviation "x" from the ideal stoichiometry in TiO_{2-x} are taken in exam (Table 2) as well.

Figure 13 shows O_{O-Ti}/Ti (i.e. O1/Ti) and Ti^{3+}/Ti^{4+} atomic ratios as function of the titanium dioxide film obtained with different number of cycles. O_{O-Ti}/Ti ratio increases increasing the number of cycles, while Ti^{3+}/Ti^{4+} atomic ratio decreases with increasing number of cycles. In both cases, the values are almost constant for a large number of deposition cycles (≥ 150 cycles), while they change rapidly following exponential curves below 150 deposition cycles (insert Fig. 13).

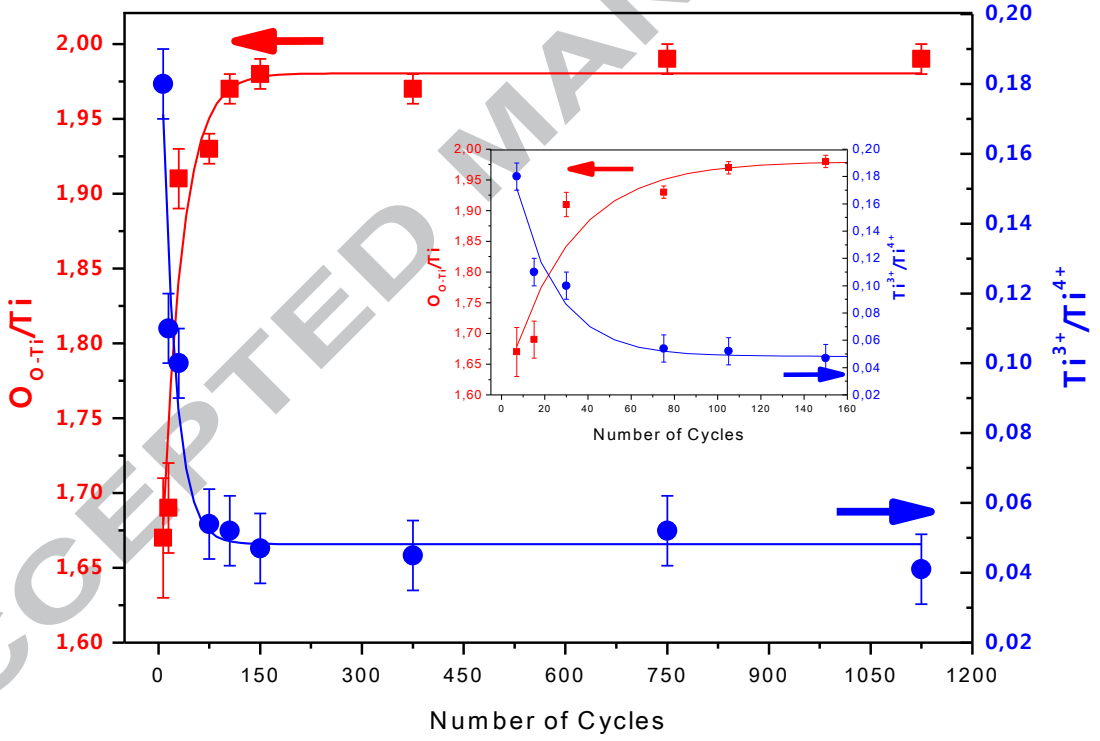

Figure 13: O_{O-Ti}/Ti (red squares) and Ti^{3+}/Ti^{4+} (blue dots) atomic ratios as function of the number of ALD cycles in the range of 0-1125 cycles and 0-150 cycles in the insert graph.

O_{O-Ti}/Ti and Ti^{3+}/Ti^{4+} atomic ratios have opposite evolution trend with film thickness increase. Ti^{3+} states of titanium can be ascribed to stoichiometry deficiency of the oxide [65],

or to the presence of a Ti_2O_3 phase [59]. From the only Ti2p peak features, it is difficult to discriminate between the one or the other case. Moreover, the O2 component of the O1s core line spectrum, which could be related to oxygen lattice of Ti_2O_3 [65], can also be due to an oxidized form of carbon or to OH group [59].

In order to explore the presence of oxygen vacancies, valence band (VB) spectrum was studied. It has been reported that oxygen vacancies in titanium dioxide, when present, give rise to a low intensity peak between the VB maximum and the Fermi level, corresponding to Ti3d state [73, 74, 75]. However, in our study, where the $O_{O\text{-}Ti}$/Ti atomic ratio values were the lowest and those of Ti^{3+}/Ti^{4+} the highest, i.e. for the thinnest films (after less than 105 cycles), the VB spectra were dominated by the Si/SiO_2 signal of the substrate underlaying the graphene layer. For thicker films (after 150 cycles and more), the acquired VB pertained to TiO_2, without any substrate contribution, but no significant signal between the VB maximum and the Fermi level could be detected, in accordance with the fact that the stoichiometry was close to the ideal value of 2.

The presence of the Ti3d peak could be observed only in the VB spectrum of the film after 150 ALD cycles, with a nominal thickness of 10 nm, as shown in Figure 14 (a spectrum smoothing was applied to reduce noise, using the adjacent-averaging method applied with 10 points). The spectrum clearly contains a peak (red solid line) at 1.2 eV below the Fermi level that has been reported to pertain to Ti3d states associated with oxygen vacancies [73, 74, 75].

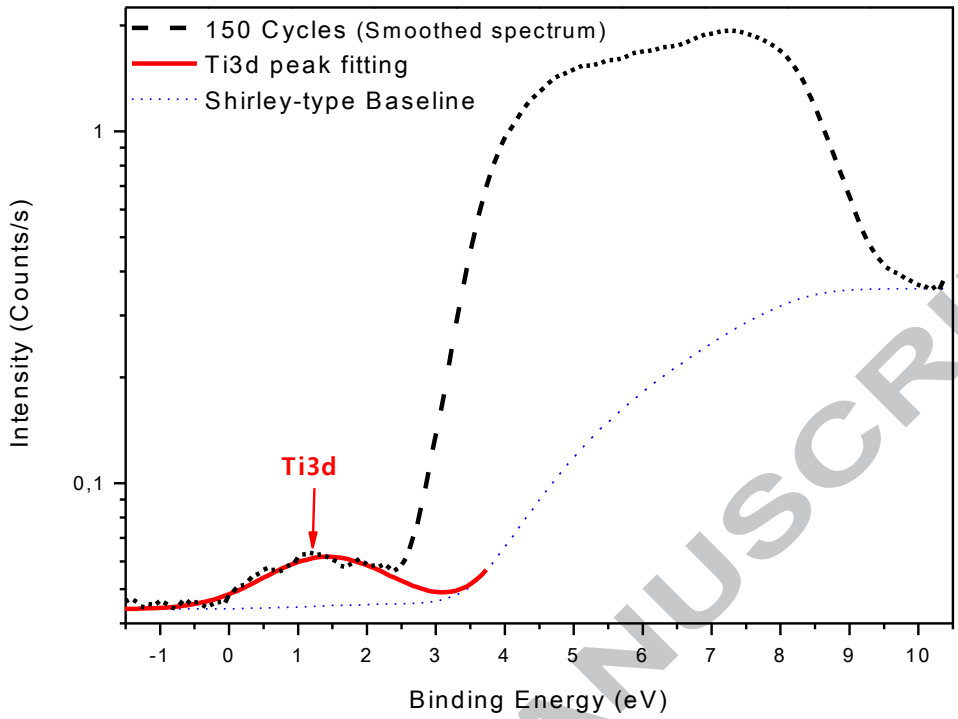

Figure 14: XPS valence band (VB) spectrum for TiO_2 film deposited onto graphene with 150 cycles. For an easier observation, the signal intensity is plotted with a logarithmic scale. The fitted peak at 1.2 eV is attributed to Ti3d state. The blue dotted line is a Shirley-type baseline. Only a fit of the Ti3d state was performed.

This result seems in contrast with the film stoichiometry ($O_{O\text{-}Ti}$/Ti ratio equal to (1.98 ± 0.01)), very close to the ideal value of 2, as it came from the Ti2p and O1s spectra. This can be understood considering that, thanks to the difference in the electron escape depth for Ti2p core line and valence band (about ~8 nm and ~10.5 nm respectively, taken as three times the inelastic mean free path determined using NIST database [72]), the analysis of a 10 nm thick film allowed to sample the film chemical structure through its whole thickness, till the interface, without significant interference of the substrate.

The results indicate that along a depth of ~8 nm from the film surface, the oxide was nearly-stoichiometric while the defected structure with oxygen vacancies concerned the remaining ~2 nm down to the interface. This depth interval compares well with the thicknesses of the nominal films after 7, 15 and 30 cycles, namely 0.5, 1 and 2 nm nominal thickness

respectively, which precisely were those with the lowest $O_{O\text{-}Ti}/Ti$ and highest Ti^{3+}/Ti^{4+} atomic ratios (Table 2).

These results show that in the thinnest films, titanium dioxide grew with an oxygen deficiency which then gradually decreased with increasing the deposition cycles number, till to achieve a full stoichiometry for a film thickness ≥ 10 nm, i.e. after more than 150 cycles. A Ti_2O_3 phase, if present, especially at the early stage of the growth, should be in a relatively negligible amount.

3.3 Photocatalytic activity

Titanium dioxide has been demonstrated to possess photocatalytic properties in the UV range [11, 12, 76].

The aim of this measurement is to verify if the presence of graphene influences the photocatalytic activity of TiO_2 in the UV-Visible range and, in particular, under the solar light irradiation range. Figure 15 shows the degradation kinetics of methyl red for TiO_2 (1125 ALD cycles), TiO_2/Graphene hybrid material (1125 ALD cycles) and untreated graphene under the exposition to a solar simulator set at the power of 1 sun. After about 5 hours (300 min ca.) TiO_2/Graphene sample shows the highest photocatalytic activity compared to TiO_2 film and graphene samples. The absorbance of the dye in contact with the TiO_2/Graphene hybrid material is reduced by a factor 10, while its reduction for TiO_2 and graphene samples is <10% with respect to the initial value. Therefore, the photocatalytic activity of TiO_2/Graphene composite is very high compared to that of TiO_2 film (deposited on silicon substrate). It is worth to notice that the TiO_2 film obtained with 1125 ALD cycles has been deposited onto the two substrates (graphene film and silicon) exactly at the same conditions.

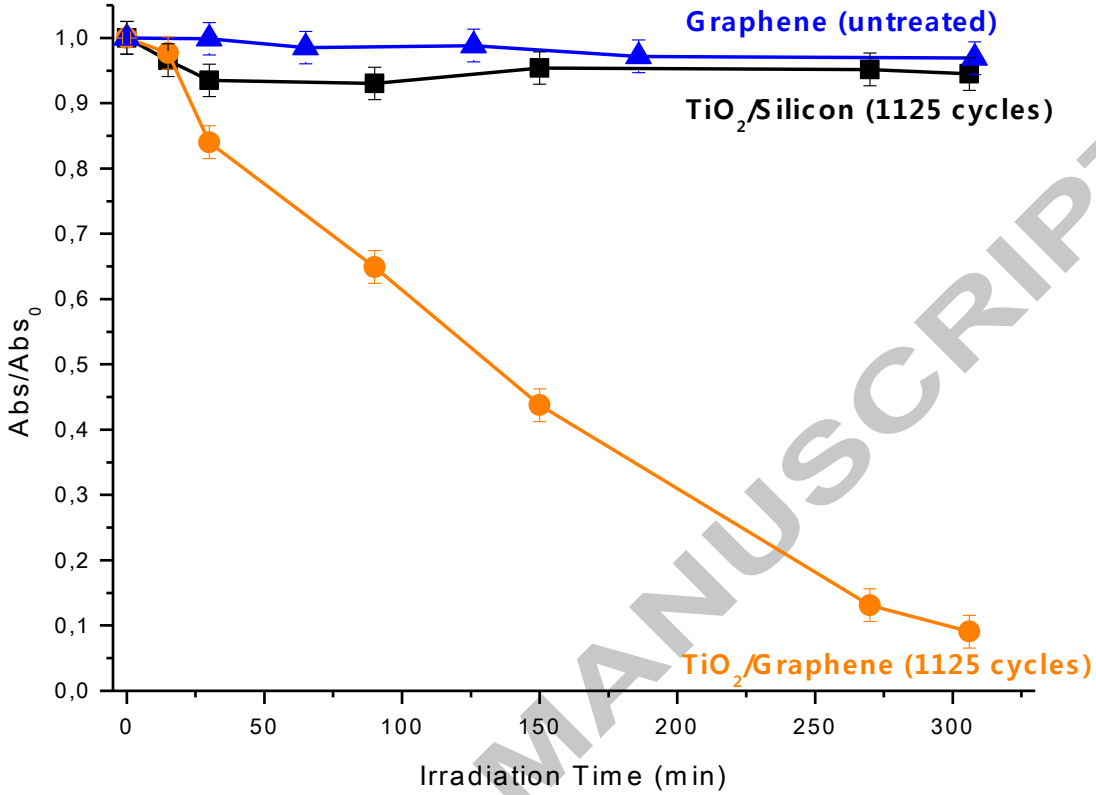

Figure 15*:* Normalized absorbance at 430 nm with respect to the value at initial time as a function of irradiation time under solar simulator (1 KW/m^2) for: TiO_2/Graphene (1125 deposition cycles, 75 nm nominal thickness) (orange dots), TiO_2 (1125 ALD cycles, 75 nm nominal thickness) (black squares) and untreated graphene sample (blue triangles).

Comparing the photocatalytic activity of graphene samples decorated with 105, 375, 750 and 1125 ALD cycles (Figure 16), it was observed that the photodegradation of the dye depends not only on the presence/absence of graphene, but also on the TiO_2 film thickness. In particular, from Figure 16 is evident that increasing the thickness of titania deposited on graphene film clearly increased the photocatalytic activity of the sample.

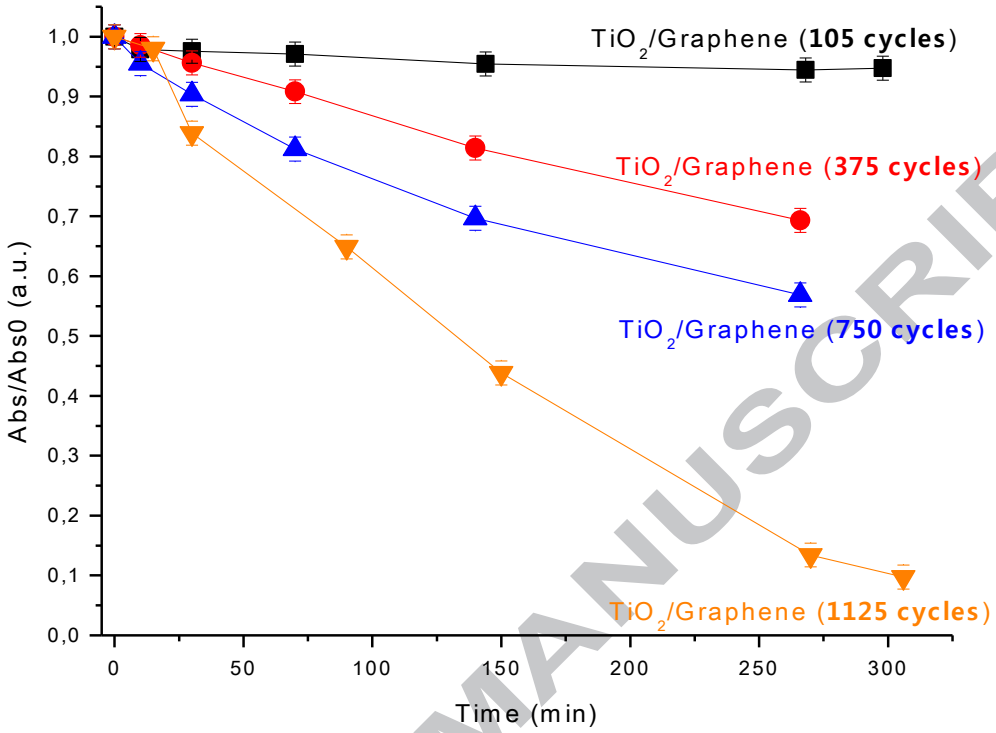

Figure 16: Normalized absorbance at 430 nm with respect to the value at initial time as a function of irradiation time under solar simulator (1 KW/m^2) for: TiO_2/Graphene decorated with 105 (black squares), 375 (red circles), 750 (blue triangles) and 1125 (orange inverted triangles) deposition cycles, which correspond to 7 nm, 25 nm, 50 nm and 75 nm nominal film thickness respectively.

The enhancement of photodegradation for TiO_2/Graphene hybrid material is reported to be due to the higher efficiency in electron-hole separation [12, 49]. In fact, the photo-generated electron in TiO_2 will move from the conduction band of titania to the (p-doped) graphene layer [12, 77, 78], while the photo-generated hole will stay in the valence band of TiO_2, minimizing the recombination rate and therefore increasing the degradation yield, since the photo-generated electron and hole can lead to reduction and oxidation reactions respectively. Increasing the quantity of TiO_2 (by increasing the number of deposition cycles), increases the number of sites where electron-hole pair can be photo-generated as well [78].

Moreover, the photocatalytic activity shifted in the UV-Visible range [49] can be explained studying the UV-Vis absorption spectrum of titania/graphene hybrid materials (Figure 17).

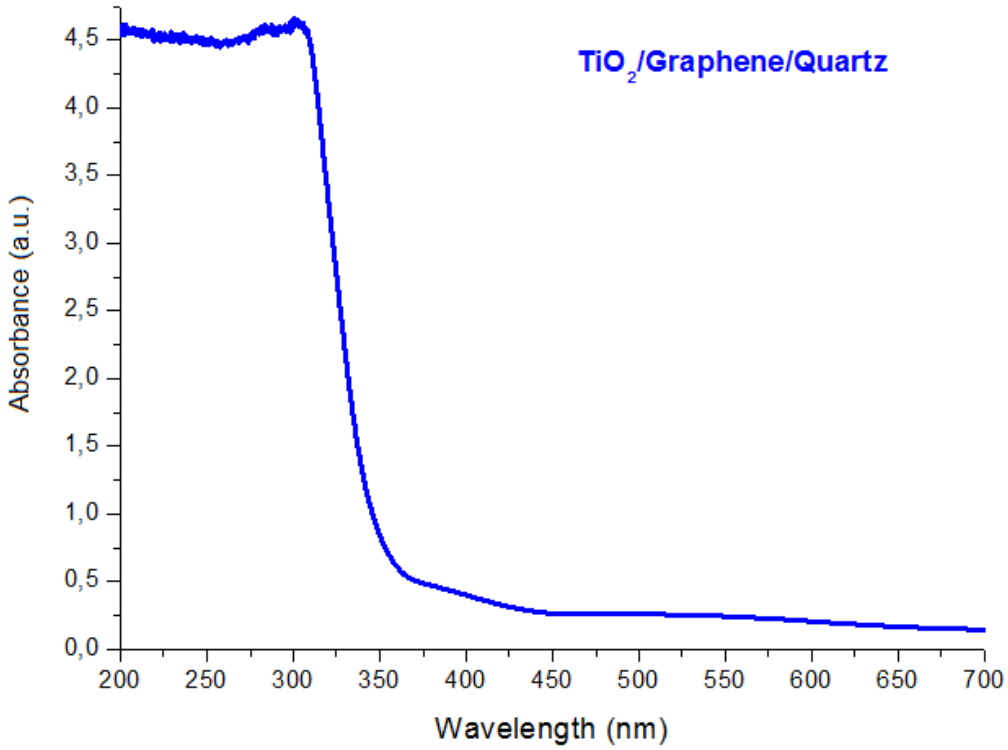

Figure 17: UV-Vis absorption spectrum of TiO_2 film deposited on graphene film (graphene film is on a quartz substrate). The wavelength range goes from 200 nm to 700 nm.

The absorbance of the hybrid material did not go to zero after the absorption edge of TiO_2 (i.e for $\lambda > 350$ nm) (it is well known that TiO_2 absorbs light only in the UV range), but it remained between 0.5 and 0.25 in the whole visible range ($350 \text{ nm} < \lambda \leq 700$ nm). This extended light harvesting capability can be ascribed to the presence of graphene [78, 79, 80, 81] and to the presence of oxygen vacancies [82, 83].

The calculation of the rate constant for TiO_2/Graphene samples was performed using the following formula, according to the first-order kinetic law [84]:

$$\frac{C}{C_0} = e^{-kt} \qquad \text{Eq. 1}$$

Where C_0 and C are the initial dye concentration and its concentration at time t respectively, while k is the rate constant. Since the absorption (Abs) is equal to Abs = εbC from the Lambert-Beer law (where ε is the molar absorbitivity, b is the path length of the sample (i.e. the path of the cuvette with the sample) and C the concentration), then $Abs/Abs_0 = C/C_0$. Therefore, the previous equation for the calculation of the rate constant can be written as follows:

$$\frac{Abs}{Abs_0} = e^{-kt} \qquad \text{Eq. 2}$$

From the exponential fitting of the data, the maximum rate constant k = (0.0064 ± 0.0006) min^{-1} was achieved for the sample decorated with 1125 deposition cycles, while k was ~ 0.0024 min^{-1} and ~ 0.0010 min^{-1} for those coated with 750 and 375 cycles respectively. It was not possible to evaluate the rate constant for untreated graphene, TiO_2/Graphene (105 cycles) and TiO_2/Silicon (1125 cycles) samples. In fact, the ~ 10% reduction in absorbance for these samples does not follow a first-order kinetic law; rather it is consistent with the degradation of the dye under the solar irradiation, i.e. the degradation of the dye for these samples is not due to the photocatalytic activity of the samples themselves.

This result shows that even though the oxygen vacancies absorb in the visible region [82], for the sample coated with 105 cycles (for which titania is not stoichiometric and the number of oxygen vacancies is not negligible, according to XPS analysis) they act as traps for photo-generated electrons. Therefore, oxygen vacancies inhibit the electron transport from TiO_2 to graphene layer [85] losing in electron-hole separation efficiency and resulting in a lower photocatalytic activity of the sample.

4. Conclusions

Graphene characteristic Raman peaks changed in shape, intensity and position when the number of ALD cycles for the deposition of TiO_2 was increased. Variations in Raman spectra

were observed also within the same sample indicating inhomogeneity and intrinsic strain effects. A study on the graphene sample (without titanium dioxide) showed that strain, caused by the mismatch with the underlying substrate, pre-existed and nonintentional self-doping was present.

Combining Raman and XPS analysis, it has been found that for a lower number of deposition cycles (≤150 cycles) a p-doping process occurred. In particular, XPS analysis showed that the lower the number of deposition cycles, the higher the oxygen vacancies quantity. This phenomenon is related to the interaction of the TiO_2 with the graphene layer in the interface region.

Increasing the number of TiO_2 deposition cycles, anatase phase appears in Raman spectra and the oxide stoichiometry was almost achieved (according to XPS analysis). The growth of the oxide film was accompanied by the creation of a tensile stress into graphene.

The photocatalytic activity test on TiO_2-Graphene sample showed that this hybrid material has a higher photocatalytic activity with respect to the TiO_2 film deposited onto a silicon substrate in the same conditions, which were both tested under a solar simulator at the power of 1 sun (UV-Vis light). At the same time increasing the titania film thickness on graphene, the photocatalytic activity was enhanced as well. TiO_2 has known photocatalytic properties in the UV range, but the incorporation of graphene enhances the overall photocatalytic performance. The TiO_2-Graphene composite, in fact, enhances both separation and transportation properties, which are fundamental in the photodegradation of pollutants.

Acknowledgements

We would like to thank Giorgio Speranza for the development of the fitting software based on RStudio used for XPS analysis.

References

[1] Virendra Singh, Daeha Joung, Lei Zhai, Soumen Das, Saiful I. Khondaker and Sudipta Seal, "Graphene based materials: past, present and future," *Progress in Materials Science 56,* pp. 1178-1271, 2011.

[2] A.C. Ferrari, "Raman spectroscopy of graphene and graphite: disorder, electron-phonon coupling, doping and nonadiabatic effects," *Solid State Communications 143,* pp. 47-57, 2007.

[3] J. C. Slonczewski and P. R. Weiss, "Band structure of graphite," *Phys. Rev. 109,* p. 272, 1958.

[4] Matthew J. Allen, Vincent C. Tung and Richard B. Kaner, "Honeycomb carbon: a review of graphene," *Chemical Reviews,* vol. 110, no. 1, pp. 132-145, 2010.

[5] C. Lee, X. Wei, J. W. Kysar and J. Hone, "Measurement of the elastic properties and intrinsic strength of monolayer graphene," *Science 321,* p. 385, 2008.

[6] A. A. Balandin, S. Ghosh, W. Bao, I. Calizo, D. Teweldebrhan, F. Miao and et al., "Superior thermal conductivity of single-layer graphene," *Nano Lett 8,* p. 902, 2008.

[7] K. S. Novoselov, A. K. Geim, S. V. Morozov, D. Jiang, M. I. Katsnelson, I. V. Grigorieva and et al., "Two-dimensional gas of massless Dirac fermions in graphene," *Nature 438,* p. 197, 2005.

[8] K.S. Novoselov, A. K. Geim, S. V. Morozov, D. Jiang, Y. Zhang, S. V. Dubonos and et al., "Electric field effect in atomically thin carbon films," *Science 306,* p. 666, 2004.

[9] Tapas Kuila, Saswata Bose, Ananta Kumar Mishra, Partha Khanra, Nam Hoon Kim and Joong Hee Lee, "Chemical functionalization of graphene and its applications," *Progress in Materials Science 57,* pp. 1061-1105, 2012.

[10] Xiangbo Meng, Dongsheng Geng, Jian Liu, Ruying Li and Xueliang Sun, "Controllable synthesis of graphene-based titanium dioxide nanocomposites by atomic layer deposition," *Nanotechnology 22,* p. 165602, 2011.

[11] Hao Zahng, Xiaojun Lv, Yueming Li, Ying Wang and Jinghong Li, "P25-Graphene composites as a high performance photocatalyst," *AcsNano 4,* pp. 380-386, 2010.

[12] Quinjun Xiang, Jiaguo Yu and Mietek Jaroniec, "Graphene-based semiconductor photocatalysts," *Chem. Soc. Rev 41,* pp. 782-796, 2012.

[13] V. Miikkulainen, M. Leskelä, M. Ritala and R. L. Puurunen, "Crystallinity of inorganic films grown by atomic layer deposition: Overview and general trends," *Journal of Applied Physics 113,* p. 021301, 2013.

[14] Steven M. George, "Atomic layer deposition: an overview," *Chem. Rev. 110,* pp. 111-131, 2010.

[15] A.K. Geim and K.S. Novoselov, "The rise of graphene," *Nature Materials,* vol. 6, pp. 183-191, March 2007.

[16] Ryan Beams, Luiz Gustavo Cançado and Lukas Novotny, "Raman characterization of defects and dopants in graphene," *Journal of Physics: Condensed Matter 27,* p. 083002, 2015.

[17] H. E. Romero, N. Shen, P. Joshi, H. R. Gutierrez, S. A. Tadigadapa, J. O. Sofo and P.C. Eklund, "n-Type behaviour of graphene supported on Si/SiO2 substrates," *ACS Nano Vol.2, No. 10,* pp. 2037-2044, 2008.

[18] Y. Xuan, Y. Q. Wu, T. Shen, M. A. Capano, J. A. Cooper and P. D. Ye, "Atomic-layer-deposited nanostructures for graphene-based nanoelectronics," *Applied Physics Letters 92,* p. 013101, 2008.

[19] Chunmei Ban, Ming Xie, Xiang Sun, Jonathan J. Travis, Gongkai Wang, Hongtao Sun, Anne C. Dillon, Jie Lian and Steven M. George, "Atomic layer deposition of amorphous TiO2 on graphene as an anode for Li-ion batteries," *Nanotechnology 24,* p. 424002 (6pp), 2013.

[20] Y. Badr, M. G. Abd El-Mahed and M. A. Mahmoud, "Photocatalytic degradation of methyl red dye by silica nanoparticles," *Journal of Hazardous Materials 154,* pp. 245-253, 2008.

[21] G. Mascolo, R. Comparelli, M. L. Curri, G. Lovecchio, A. Lopez and A. Agostiano, "Photocatalytic degradation of methyl red by TiO2: comparison of the efficiency of immobilized nanoparticles versus conventional suspended catalyst," *Journal of Hazardous Materials 142,* pp. 130-137, 2007.

[22] W. F. Zhang, Y. L. He, M. S. Zhang, Z. Yin and Q. Chen, "Raman scattering study on anatase TiO2 nanocrystals," *Journal of Physics D: Applied Physics 33,* pp. 912-916, 2000.

[23] Jaan Aarik, Aleks Aidla, Teet Uustare and Väino Sammelselg, "Morphology and structure of TiO2 thin films grown by atomic layer deposition," *Journal of Crystal Growth 148,* pp. 268-275, 1995.

[24] Isaac Childres, Luis A. Jauregui , Jifa Tian and Yong P. Chen, "Effect of oxygen plasma etching on graphene studied using Raman spectroscopy and electronic transport measurements," *New Journal of Physics 13,* p. 025008, 2011.

[25] L.G. Cançado, A. Jorio, E.H. Martins Ferreira, F. Stavale, C.A. Achete, R.B. Capaz, M.V.O. Moutinho, A. Lombardo, T. Kulmala and A.C. Ferrari, "Quantifying defects in graphene via Raman spectroscopy at different excitation energies," *Nano Lett. 11,* pp. 3190-3196, 2011.

[26] I. Childres, L.A. Jauregui, W. Park, H. Cao and Y.P. Chen, "Raman spectroscopy of graphene and related materials," in *Developments in photon and materials research*, Jang JI, 2013.

[27] A. C. Ferrari, J. C. Mayer, V. Scardaci, C. Casiraghi, M. Lazzeri, F. Mauri, S. Piscanec, D. Jiang, K. S. Novoselov, S. Roth and A. K. Geim, "Raman spectrum of graphene and graphene layers," *Physical Review Letters 97,* p. 187401, 2006.

[28] L. M. Malard, M.A. Pimenta, G. Dresselhaus and M. S. Dresselhaus, "Raman spectroscopy in graphene," *Physics Reports 473,* pp. 51-87, 2009.

[29] S. Pisana, M. Lazzeri, C. Casiraghi, K.S. Novoselov, A.K. Geim, A.C. Ferrari and F. Mauri, "Breakdown of the adiabatic Born-Oppenheimer approximation in graphene," *Nature Materials,* vol. 6, pp. 198-201, March 2007.

[30] C. Casiraghi, S. Pisana, K.S. Novoselov, A.K. Geim and A.C. Ferrari, "Raman fingerprint of charged impurities in graphene," *Applied Physics Letters 91,* p. 233108, 2007.

[31] A. Jorio, R. Saito, G. Dresselhaus and M. S. Dresselhaus, Raman spectroscopy in graphene related system, Wiley-VCH, 2011.

[32] Y. Shi, X. Dong, P.Chen, J. Wang and L. Li, "Effective doping pf single-layer graphene from underlying SiO2 substrates," *Physical review B 79,* p. 115402, 2009.

[33] A. C. Ferrari and J. Robertson, "Resonant Raman spectroscopy of disordered, amorphous, and diamondlike carbon," *Physical Review B,* vol. 64, p. 075414, 2001.

[34] A. Das, B. Chakraborty and A. K. Sood, "Raman spectroscopy of graphene on different substrates and influence of defects," *Bulletin of Material Science 3,* vol. 31, pp. 579-584, 2008.

[35] T. M. G. Mohiuddin, A. Lombardo, R. R. Nair, A. Bonetti, G. Savini, R. Jalil, N. Bonini, D.M. Basko, C. Galiotis, N. Marzari, K. S. Novoselov, A. K. Geim and A. C. Ferrari, "Uniaxial strain in graphene by Raman Spectroscopy: G peak splitting, Gruneisen parameters and sample orientation," *Physical Review B 79,* p. 205433, 2009.

[36] O. Frank, G. Tsoukleri, J. Parthenios, K. Papagelis, I. Riaz, R. Jalil, K. S. Novoselov and C. Galiotis, "Compression behavior of single-layer graphene," *ASC Nano 4,* pp. 3131-3138, 2010.

[37] Dong Su Lee, Christian Riedl, Benjamin Krauss, Klaus von Klitzing, Ulrich Starke and Jurgen H. Smet, "Raman spectra of epitaxial graphene on SiC and of epitaxial graphene transferred on SiO2," *Nano Letters Vol. 8, No. 12,* 2008.

[38] Q. H. Wang, Z. Jin, K. K. Kim, A. J. Hilmer, G. L. C. Paulus, C. J. Shih, M. H. Ham, J. D. Sanchez-Yamagishi, K. Watanabe, T. Taniguchi, J. Kong, P. Jarillo-Herrero and M. S. Strano,

"Understanding and controlling the substrate effect on graphene electron-transfer chemistry via reactivity imprint lithography," *Nature Chemistry, vol. 4,* September 2012.

[39] Z. Luo, C. Cong, J. Zhang, Q. Xiong and T. Yu, "The origin of sub-bands in Raman D-band of graphene," *Carbon, 50,* pp. 4252-4258, 2012.

[40] E. H. Martins Ferreira, Marcus V. O. Moutinho, F. Stavale, M. M. Lucchese, Rodrigo B. Capaz, C. A. Achete and A. Jorio, "Evolution of the Raman spectra from single, few and many layers graphene with increasing disorder," *Physical Review B, Condensed Matter and Materials Physics, Vol. 82, Issue 12,* 2010.

[41] Xinyu Wang, Jie Zhang, Xiaolei Zhang and Yong Zhu, "Characterization, uniformity and photocatalytic properties of graphene/TiO2 composites via Raman mapping," *Optics Express Vol.25, No.18,* 2017.

[42] A. Das, S. Pisana, B. Chakraborty, S. Piscanec, S. K. Saha, U. V. Waghmare, K. S. Novoselov, H. R. Krishnamurthy, A. K. Geim, A. C. Ferrari and A. K. Sood, "Monitoring dopants by Raman scattering in an electrochemically top-gated graphene transistor," *Nature Nanotechnology Vol.3,* pp. 210-215, April 2008.

[43] M. B. B. S. Larsen, D. M. A. Mackenzie, J. M. Caridad, P. Bøggild and T. J. Booth, "Transfer induced compressive strain in graphene: evidence from Raman spectroscopic mapping," *Microelectronic Engeneering 121,* pp. 113-117, 2014.

[44] J. E. Lee, G. Ahn, J. Shim, Y. S. Lee and S. Ryu, "Optical separation of mechanical strain from charge doping in graphene," *Nature Comunications 3,* p. 1024, 2012.

[45] K. Filintoglou, N. Papadopoulos, J. Arvanitidis, D. Christofolos, O. Frank, M. Kalbac, J. Parthenios, G. Kalosakas, C. Galiotis and K. Papagelis, "Raman spectroscopy of graphene at high pressure: effects of the substrate and the pressure trasmitting media," *Physical Review B 88,* p. 045418, 2013.

[46] Mark A. Bissett, Masaharu Tsuji and Hiroki Ago, "Strain engineering the properties of graphene and other two-dimensional crystals," *Phys. Chem. Chem. Phys 16,* pp. 11124-11138, 2014.

[47] F. Schedin, A. K. Geim, S. V. Morozov, E. W. Hill, P. Blake, M. I. Katsnelson and K. S. Novoselov, "Detection of individual gas molecules adsorbed on graphene," *Nature Materials Vol 16,* pp. 652-655, September 2007.

[48] H. Liu, Y. Liu and D. Zhu, "Chemical doping of graphene," *Journal of Materials Chemistry 21,* pp. 3335-3345, 2011.

[49] A. Du, Y. H. Ng, N. J. Bell, Z. Zhu, R. Amal and S. C. Smith, "Hybrid graphene/titania nanocomposite: interface charge transfer, hole doping, and sensitization for visible light response," *J. Phys. Chem. Lett. 2 (8),* pp. 894-899, April 2011.

[50] A. Pirkle, J. Chan, A. Venugopal, D. Hinojos, C. W. Magnuson, S. McDonnell, L. Colombo, E. M. Vogel, R. S. Ruoff and R. M. Wallace, "The effect of chemical residues on the physical and electrical properties of chemical vapor deposited graphene transferred to SiO2," *Applied Physics Letters 99,* p. 122108, 2011.

[51] S. Ryu, S. Berciaud, Y. Yu, H. Liu, P. Kim, G. W. Flynn and L. E. Brus, "Atmospheric oxygen binding and hole doping in deformed graphene on a SiO2 substrate," *Nano Letters 10,* pp. 4944-4951, 2010.

[52] K. Röll, "Analysis of stress and strain distribution in thin films and substrates," *Journal of Applied Physics 47,* p. 3224, 1976.

[53] R. C. Cammarata, T. M. Trimble and D. J. Srolovitz, "Surface stress model for intrinsic stresses in thin films," *Journal of Materials Research Vol 15, Issue 11,* pp. 2468-2474, November 2000.

[54] C. Pannu, U. B. Singh, S. Kumar, A. Tripathi, D. Kabiraj and D. K. Avasthi, "Engineering the strain in graphene layers with Au decoration," *Applied Surface Science Vol. 308,* pp. 193-198, 30 July 2014.

[55] V. Micheli, N. Laidani, R. Bartali, G. Gottardi and M. Anderle, "Interface effects study in hard–soft carbon multilayered films by AES depth profiling," *Plasma Processes and Polymers 4,* pp. S259-S264, 2007.

[56] U. Diebold, "The surface science of titanium dioxide," *Surface Science Reports 48,* pp. 53-229, 2003.

[57] John F. Moulder, William F. Stickle, Peter E. Sobol and Kenneth D. Bomben, Handbook of X-ray Photoelectron Spectroscopy, Physical electronics Inc., 1995.

[58] Yongqing Fu, Hejun Du, Sam Zhang and Weimin Huang, "XPS characterization of surface and interfacial structure of sputtered TiNi films on Si substrate," *Materials Science and Engineering A 403,* pp. 25-31, 2005.

[59] A. C. Bronneberg, C. Höhn and R. van de Krol, "Probing the interfacial chemistry of ultrathin ALD-grown TiO2 films: an in-line XPS study," *The Journal of Physical Chemistry C 121,* pp. 5531-5538, 2017.

[60] B. J. Morgan and G. W. Watson, "Intrinsic n-type defect formation in TiO2: a comparison of rutile and anatase form GAA+U calculations," *Journal of Physical Chemistry C 114,* pp. 2321-2328, 2010.

[61] Y. Cai, Z. Bai, S. Chintalapati, Q. Zeng and Y. P. Feng, "Transition metal atoms pathways on rutile TiO2 (110) surface: distribution of Ti3+ states and evidence of enhanced peripheral charge accumulation," *The Journal of Chemical Physics 138,* p. 154711, 2013.

[62] F. Banhart, J. Kotakoski and A. V. Krasheninnikov, "Structural defects in graphene," *ACS Nano vol.5, no.1,* pp. 26-41, 2011.

[63] B. Bharti, S. Kumar, H.-N. Lee and R. Kumar, "Formation of oxygen vacancies and Ti3+ state in TiO2 thin film and enhanced optical properties by air plasma treatment," *Scientific Reports 6,* p. 32355, 2016.

[64] M.V. Kuznetsov, Ju. F. Zhuravlev and V.A. Gubanov, "XPS analysis of adsorption of oxygen molecules on the surface of Ti and TiNx films in vacuum," *Journal of Electron Spectroscopy and Related Phenomena 58,* pp. 169-176, 1992.

[65] I. Luciu, R. Bartali and N. Laidani, "Influence of Hydrogen addition to an Ar plasma on the structural properties of TiO2-x thin films deposited by RF sputtering," *Journal of Physics D: Applied Physics 45,* p. 345302 (9pp), 2012.

[66] D. O. Scanlon, C. W. Dunnill, J. Buckeridge, S. A. Shevlin, A. J. Logsdail, S. M. Woodley, C. R. A. Catlow, M. J. Powell, R. G. Palgrave, I. P. Parkin, G. W. Watson, T. W. Keal, P. Sherwood, A. Walsh and A. A. Sokol, "Band allignment of rutile and anatase TiO2," *Nature Materials 12,* pp. 798-801, 2013.

[67] Gang Xiong, Rui Shao, Timothy C. Droubay, Alan G. Joly, Kenneth M. Beck, Scott A. Chambers and Wayne P. Hess, "Photoemission electron microscopy of TiO2 anatase films embedded with rutile nanocrystals," *Advanced functional materials 17,* pp. 2133-2138, 2007.

[68] Zhenyu Chen, Iman Santoso, Rui Wang, Lan Fei Xie, Hong Ying Mao, Han Huang, Yu Zhan Wang, Xing Yu Gao, Zhi Kuan Chen, Dongge Ma, Andrew Thye Shen Wee and Wei Chen, "Surface transfer hole doping of epitaxial graphene using MoO3 thin film," *Applied Physics Letters 96,* p. 213104, 2010.

[69] J. Meyer, P. R. Kidambi, B. C. Bayer, C. Weijtens, A. Kuhn, A. Centeno, A. Pesquera, A. Zurutuza, J. Robertson and S. Hofmann, "Metal oxide induced charge transfer doping and band alignment of graphene electrodes for efficient orghanic light emitting diodes," *Scientific Reports 5380,* 2014.

[70] Zhen Zhang and John T. Yates, Jr., "Band bending in semiconductors: Chemical and Physical consequences at surfaces and interfaces," *Chemical Reviews 112,* pp. 5520-5551, 2012.

[71] A. El-Sayed, P. Borghetti, E. Goiri, C. Rogero, L. Floreano, G. Lovat, J. L. Cabellos, Y. Wakayama,

A. Rubio, J. E. Ortega, D. G. de Oteyza and D. J. Mowbray, "Understanding energy-level alignment in donor-acceptor/metal interfaces from core-level shifts," *ACS Nano Vol.7, No.8,* pp. 6914-6920, 2013.

[72] C. J. Powell and A. Jablonski, *NIST Standard Reference database 82, Electron Effective Attenuation Length Database, version 1.0, National Institute of Standards & technology, Gaithersburg, MD,* 2001.

[73] N. Laidani, P. Cheyssac, J. Perrière, R. Bartali, G. Gottardi, I. Luciu and V. Micheli, "Intrinsic defects and their influence on the chemical and optical properties of TiO2-x films," *Journal of Physics D: Applied Physics 43,* p. 485402 (11pp), 2010.

[74] M. Hannula, H. Ali-Löytty, K. Lahtonen, E. Sarlin, J. Saari and M. Valden, "Improved stability of atomic layer deposited amorphous TiO2 photoelectrode coatings by thermally induced oxygen defects," *Chemistry of Materials 30,* pp. 1199-1208, 2018.

[75] C. Di Valentin, G. Pacchioni and A. Selloni, "Reduced and n-type doped TiO2: nature of Ti3+ species," *J. Phys. Chem. C 113,* pp. 20543-20552, 2009.

[76] Yoshihiko Ohama and Dionys Van Gemert, Application of titanium dioxide photocatalysis to construction materials, Springer, 2011.

[77] M. Xing, F. Shen, B. Qiu and J. Zhang, "Highly-dispersed boron-doped graphene nanosheets loades with TiO2 nanoparticles for enhancing CO2 photoreduction," *Scientific Reports 6341,* September 2014.

[78] Y. Zhang, Z. R. Tang, X.Fu and Y. J. Xu, "TiO2-Graphene nanocomposites for gas-phase photocatalytic degradation of volatile aromatic pollutat: is TiO2-Graphene truly different from other TiO2-Carbon composites materials?," *ACS Nano Vol.4, No. 12,* p. 7303+7314, 2010.

[79] K. Palanivelu, Ji Sun Im and Young-Seak Lee, "Carbon doping of TiO2 for visible light photo catalysis-a review," *Carbon Science,* vol. 8, no. 3, pp. 214-224, 2007.

[80] F. Zabihi, M. R. Ahmadian-Yazdi and M. Eslamian, "Photocatalytic graphene-TiO2 thin films fabricated by low temperature ultrasonic vibration-assisted spin and spry coating in a sol-gel process," *Catalysts 7,* p. 136, 2017.

[81] Y. Zhang and C. Pan, "TiO2/graphene composite from thermal reaction of graphene oxide and its photocatalytic activity in visible light," *Journal of Materials Science 46,* pp. 2622-2626, 2011.

[82] D. Li, H. Haneda, N. K. Labhsetwar, S. Hishita and N. Ohashi, "Visible-light-driven photocatalysis on fluorine-doped TiO2 powders by the creation of surface oxygen vacancies," *Chemical Physics Letters 401,* pp. 579-584, 2005.

[83] I. Nakamura, N. Negishi, S. Kutsuna, T. Ihara, S. Sugihara and K. Takeuchi, "Role of oxygen vacancy in the plasma-treated TiO2 photocatalyst with visible light activity fo NO removal," *Journal of Molecular Catalysis 161,* pp. 205-212, 2000.

[84] H. Al-Ekabi and N. Serpone, "Photocatalytic degradation of chlorinated phenols in aerated aqueous solutions over TiO2 supported on a glass matrix," *The Journal of Physical Chemistry ,* vol. 92, no. 20, 1988.

[85] J. Wang, Z. Wang, B. Huang, Y. Ma, Y. Liu, X. Quin, X. Zhang and Y. Dai, "Oxygen Vacancy Induced Band-Gap Narrowing and Enhanced Visible Light Photocatalytic Activity of ZnO," *ACS Applied Materials and Interfaces 4,* pp. 4024-4030, 2012.

Highlights:

1- Graphene-TiO2 composite materials obtained by growing TiO2 onto graphene by means of ALD were characterized in terms of strain and doping.

2- Graphene-TiO2 composite materials obtained by growing TiO2 onto graphene by means of ALD were tested for their photo-activity under solar light.

3- High activity for organic molecule degradation demonstrated by the TiO2-graphene composite, exceeding by about ten times that of ALD TiO2 onto silicon substrates.